Developing a neutronic model of the MHTGR-350 SMR for regulatory research

B Makhubedu

orcid.org/ 0000-0002-7352-4847

Dissertation accepted in fulfilment of the requirements for the degree *Master of Science in Engineering Sciences with Nuclear Engineering* at the North-West University

Supervisor: Prof VV Naicker

Co-supervisor: Miss GP Nyalunga

Graduation: October 2025

DECLARATION

I Bontle Makhubedu declare herewith that the dissertation entitled "Developing a neutronic model of the MHTGR-350 SMR for regulatory research," which I herewith submit to the North-West University, is in compliance/partial compliance with the requirements set for the degree Master of Science in Nuclear Engineering is my own work, has been text-edited in accordance with the requirements and has not already been submitted to another university.

ACKNOWLEDGEMENTS

I dedicate and owe my journey to God. His abundant grace has carried me to where I am now. I will always be grateful for the abundant mercy given to me, the strength I never knew I needed to carry out my achievements during my academic journey.

In addition, my dedication extends to my family for the endless love and support they have shown me. My resilience has been the result of their motivation.

My supervisor and co-supervisor, Prof. Vishana Naicker and Dr. Gezekile Nyalunga, have never shown or installed any sign of doubt with my capabilities; instead, I have been given guidance, patience, and grace despite the demanding final days of my research.

Lastly, my final dedication goes to myself for remaining confident and resilient through it all. I told myself I will and I successfully did it through every hardship I have faced.

This milestone stands as a reminder of the collective effort support and belief that have been continued.

ABSTRACT

The Modular High-Temperature Gas-Cooled Reactor (MHTGR-350) is a Generation-IV small modular reactor that incorporates advanced safety features, high efficiency with high temperatures, and scalability compared to older nuclear reactors. These types of Generation-IV reactors were implemented to avoid repetitions of nuclear disasters like the Chernobyl disaster. Numerous research studies have been conducted on these types of reactors to increase their reliability and to adhere to the safety requirements established by the IAEA. This study aligns with the enhancement of safety in nuclear reactors by performing a neutronic analysis for the MHTGR-350 prismatic design for regulatory research. The use of theoretical and computational calculations was used to analyse the effect of temperature modifications on safety parameters such as the temperature coefficients of the fuel and moderator. These are the two parameters that were used in this study to analyse the behaviour of the reactor when temperatures of the materials in the model that directly affect the behaviour of the reactor are changed. Before the calculations were performed, verification of the Serpent and KENO-VI model was carried out and the results showed that the KENO-VI model could not be run to completion, resulting in the use of the Serpent model to carry out the aim of this study. The fuel reactivity coefficient was negative and the moderator reactivity coefficient was slightly positive and showed that using a difference of 5 to calculate the value was adequate. A literature source shows that a slightly positive value for the moderator reactivity coefficient can be expected for graphite reactors. The effect of the problem for radius and height for neutronic calculations was also shown to be important.

The study has tested the hexagonal structure modelling in version 3 of North-West University Reactor Code Suite (NWURCS) which was not carried out thus far in other studies of the research group. It has shown that while Serpent calculations produced consistent results, the KENO-VI model still needs to be developed, so that the “neutron leakage” of the geometry is fixed.

This work is not intended to be used directly in a safety analysis report; rather, it serves as a starting point in neutronic regulatory research for this type of reactor for the research group. To expand the study, more safety parameters should be included together with thermal fluid coupling. Transient studies should also be considered.

Key terms: Effective Multiplication Factor, Error Analysis, Small Modular Reactor, Neutronics, Neutron Flux, Reactivity coefficients, Temperature Coefficients, Monte Carlo Methods, Serpent model, KENO-VI model.

TABLE OF CONTENTS

LIST OF TABLES

LIST OF FIGURES

LIST OF ABBREVIATIONS

AEC	Atomic Energy Commission
BWR	Boiling-water Reactor
CEA	Commissariat à l'énergie atomique et aux énergies alternatives
CNPP	Chernobyl Nuclear Power Plant
Cr	Chromium
FHR	Flouride-salt-cooled High-temperature Reactors.
HTGR	High-temperature Gas-cooled Reactor
IAEA	International Atomic Energy Agency
LANL	Los Alamos National Laboratory
LWT	Light Water Reactor
MCN	Monte Carlo Neutron Transport
MCNP	Monte Carlo N-Particle
MCP	Monte Carlo Particles
MCS	Monte Carlo Simulation
NRC	Nuclear Regulatory Commission
NWU	North-West University
NWURCS	North-West University Reactor Code Suite
ORNL	Oak Ridge National Laboratory
RBMK	Reactor Belshey Moschnosti Kanalnyy
TMI	Three Mile Island

TRISO	Tristructural Isotropic fuel
UCO	Uranium Carbide Oxide
VTT	Valtion Teknillinen Tutkimuskeskus
WCR	Water-cooled Reactor

LIST OF SYMBOLS

ρ	Reactivity coefficient
σ	Standard deviation
k_{eff}	Multiplication factor
α	Temperature coefficient
T	Temperature
Chemical Formulae	
He	Helium
B	Boron
C	Carbon
O	Oxygen
Si	Silicon
SiC	Silicon Carbide
U	Uranium
$U0_2$	Uranium Oxide
UCO	Uranium Carbide Oxide

Definition of key concepts

Fuel Temperature Coefficient	The extent to which the reactivity is affected by the change in the temperature of the fuel (Lamarsh & Baratta, 2014).
Moderator Temperature coefficient	The extent to which the reactivity is affected by the change in the temperature of the moderator (Lamarsh & Baratta, 2014).
Multiplication factor	A factor that is determined by parameters that are dependent on temperature (Lamarsh & Baratta, 2014).
Neutron flux	Number of neutrons passing through a target/unit area per second (Lamarsh & Baratta, 2014).
Source Convergence	The iteration process of stabilising the fission source distribution (Cheng et al., 2024).

CHAPTER 1 INTRODUCTION

1.1 Rationale

Danielle quotes the definition of advanced nuclear reactors in Arostegui (2019) as ”a nuclear fission reactor with significant improvements over the most recent generation of nuclear fission reactors”. This definition applies to the advancement of small modular reactors. However, the history of nuclear accidents has given a negative reputation for nuclear energy, forcing stringent measures for licensing requirements (Gu, 2018).

1.2 Background (stringent safety measures)

The three major nuclear accidents that have influenced the deployment of nuclear power are discussed in this section to help understand the reasons for the improved safety measures taken in the design of the Modular High-Temperature Gas-Cooled Reactor (MHTGR-350). These safety limits help mitigate the chances of nuclear accidents and the damages caused by the aftereffects.

Chernobyl accident,

The Chernobyl accident occurred on the 26th of April, 1986 and was labelled the worst nuclear disaster in the history of nuclear accidents (IAEA, 2005) . As explained by IAEA (2005) the cause of the accident was the power plant in Ukraine that lost control after a test at a lower power was carried out. In addition, the same report by the IAEA states that this resulted in an explosion and fire that destroyed a reactor building, leading to the release of radiation into the atmosphere.

There were seven fatalities when the accident occurred, 237 firefighters and employees of Chernobyl Nuclear Power Plant (CNPP) were examined for acute radiation sicknesses after the accident, and 134 people displayed high levels of tissue damage (Saenko et al., 2011). This signalled a huge loss of human life.

Evacuations were made during the disaster, and the area was cleaned. Later, it was reported that Scandinavia and neighbouring countries were affected by radiation (Saenko et al., 2011).

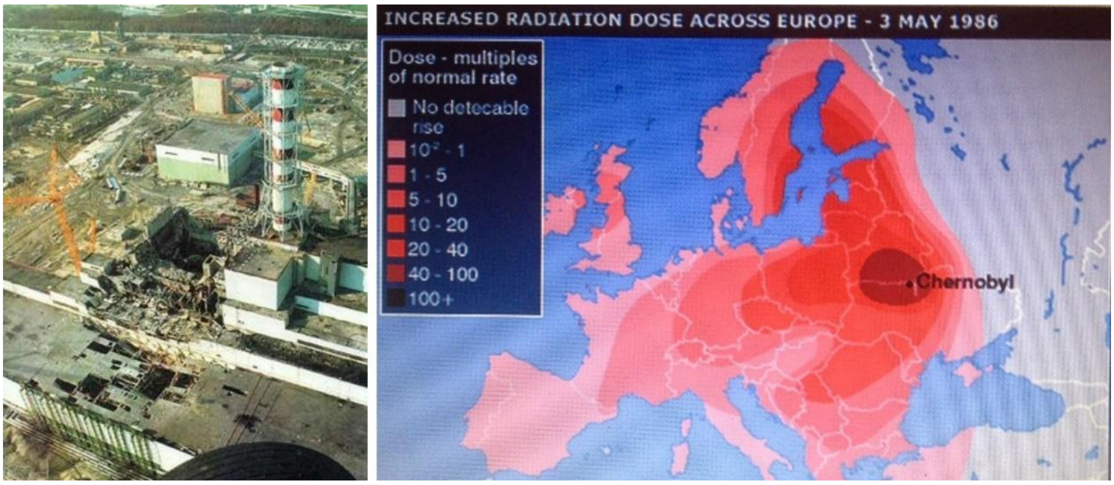

Figure 1-1: Aerial view of the destroyed reactor, 1986 (<u>left</u>), and radioactive cloud (<u>right</u>) (Origins, 2024).

Fukushima Daichii accident

The Fukushima Daichii accident was a result of an earthquake that was accompanied by a tsunami on the 11th of March, 2011 in Japan (IAEA, 2019). In summary, waves of heights greater than 10 meters were produced by the tsunami and caused the loss of power at the Fukushima Daiichi power plant. Due to this power loss, cooling systems of several reactors failed, three of which had undergone meltdowns and released radioactive materials into the atmosphere.

This prompted the evacuation of people living in and around that area, raising concerns about nuclear safety.

Figure 1-2: Radiation analysis of the sample soil (Physics OpenLab, 2017)

Three Mile Island

This accident occurred on the 28th of March, 1979 (U.S.NRC, 2022). According to the NRC report, the accident started as a failure in the cooling system and progressed to an automatic shutdown due to false information being interpreted by the operators.

About two million people were reported to have been affected by radiation. Months following the accident, vegetation was tested and monitored to show very low levels of radionuclides.

Figure 1-3: Three Mile Island after-effects (The Daily Beast, 2017)**.**

All the accidents discussed above have different causes, but the results remain the same. Radiation is a concern when it comes to nuclear energy. This concern has led to the design of reactors needing to adhere to more stringent requirements, with modular high-temperature gas-cooled reactors being one of them. In addition to the results of the accidents, the researchers were encouraged to do more research on regulatory work to assist in the practice of more stringent safety measures.

1.3 High-Temperature Gas-Cooled Reactors (HTGR)

The study on high-temperature gas-cooled reactors began in the mid-20th century; they started operating fully in 1966 (Brey, 2001). These advanced high-temperature reactors were designed with passive safety features which allowed shielding of their surroundings from the release of radioactive materials (U.S. Department of Energy).

Before discussing the implemented safety features of the HTGR, it is important to differentiate between the two types of HTGR and understand their designs. As seen in Figures 1-4, there is the Pebble Bed design and the Prismatic design.

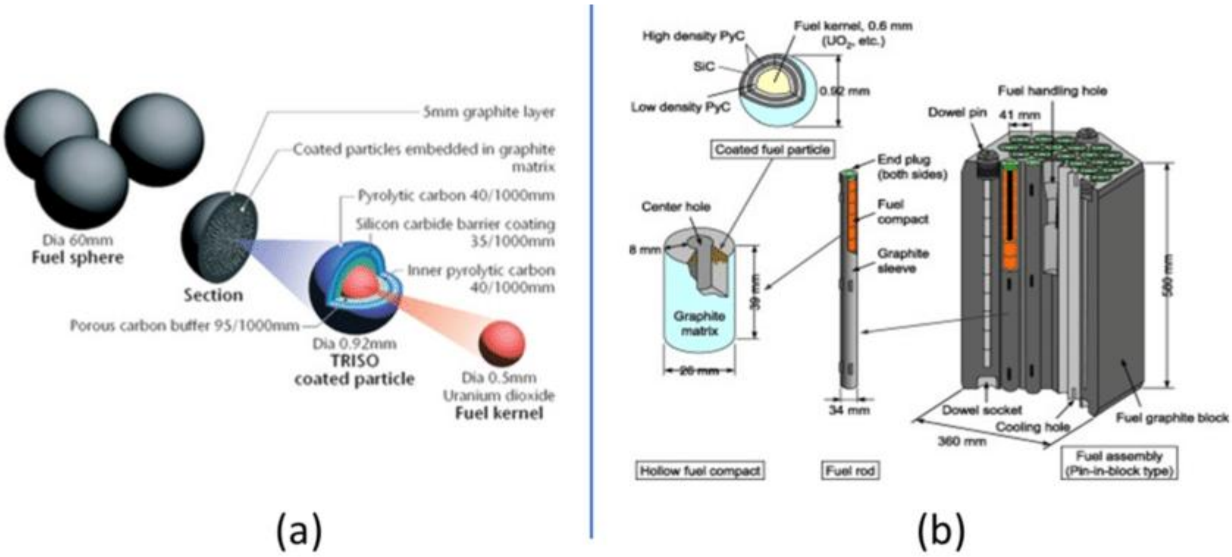

Figure 1-4: Two different forms of HTGR; (a) Pebble bed design, (b) Prismatic design (Pratama & Irwanto, 2020)**.**

The two designs are seen in terms of the environment in which the TRISO coated particles are stored. Considering the pebble-bed design, there are particles that are embedded in a spherical graphite matrix, enclosed with a spherical graphite layer, and these are known as fuel spheres. For the prismatic design, there are TRISO-coated particles embedded in cylindrical graphite matrix material to create cylindrical compacts that are then stacked on top of each other to create a 'fuel rod'. These cylindrical fuel compacts are then placed inside hexagonal graphite block fuel elements. This study focuses on the prismatic block design.

The design of the pebble-bed is being studied in another project of the North-West Universities Nuclear Engineering Department's research group, with the outcome expected to be a comparison of the two designs.

Several safety features have been implemented for both designs; a few of those safety features include spherical fuel particles with four protective layers of coating and the use of helium gas as a coolant. The use of the helium gas was because it is inert, and it is a gas known to have a relatively high heat transfer efficiency. When leaked from the primary pressure boundary, it will not condense but instead result in high pressure inside the sealed confinement that cannot be lowered by cooldown (INL, 2011).

1.4 Problem Statement

South Africa will most likely consider the deployment of high-temperature gas-cooled reactors in its new construction programme. Given the history of the Pebble-Bed Modular Reactor (PBMR) in South Africa, the SMR reactor chosen could be a pebble-bed reactor. The research group in the Nuclear Engineering Department, at North-West University (NWU) is currently involved in a project focused on this reactor type. However, the prismatic High-Temperature Gas-Cooled reactor (HTGR) type can also be considered as an HTGR choice. Hence, this choice of reactor is also considered as the reactor design chosen for this study.

When deploying a nuclear reactor in a country, adequate regulations must be in place, which in South Africa is carried out by the National Nuclear Regulator (NNR). However, given that HTGRs have not been deployed in South Africa, the licensing and operating regulations must be implemented, and incorporated into the guidelines of the NNR.

Such a task is a massive undertaking and contains many aspects to consider, such as legal regulations, physical experiments and tests, and computational analysis. Within computational analysis, many fields also need to be considered, such as structural analysis, fuel performance, neutronic calculations, etc.

Given the limited time constraints of a Masters study, this study therefore only serves to address one aspect of what is mentioned above, which is the neutronic analysis of the reactor core. In addition, it serves as a starting point for research in this field.

1.5 Aim

The aim of the study was to perform a neutronic analysis of two safety parameters for the MHTGR-350 to contribute to regulatory research.

1.6 Objectives

The aim was reached using the six objectives listed below:

1. Identifying two neutronic safety parameters on which to perform the analysis,
2. Getting the theoretical formulation for calculating these parameters,
3. Running and verifying the full core Serpent base model as generated using NWURCS,

4. Running and verifying KENO-VI models by comparing them with the Serpent models,
5. Calculating the safety parameters with the errors using the base model,
6. Comparing these results with the values for other HTGR analyses,

1.7 Acknowledgement

We appreciate the financial support provided by the National Nuclear Regulator (NNR) through the Centre for Nuclear Safety and Security (CNSS) for the research work carried out. The NNR is not held liable for any of the results, outcomes and/or shortcomings of this study.

1.8 Chapter summary

The first chapter of this dissertation outlined the rationale and purpose for this kind of research by including the background of nuclear energy and the negative connotation it has built for itself. This delved deeper into the background of HTGR being designed to mitigate some of the issues that have been raised in nuclear energy. The chapter does not only focus on the background but also portrays the framework on how the aim of this dissertation will be carried out, while acknowledging the support given by the NNR for making this study possible.

CHAPTER 2 REACTOR THEORY AND LITERATURE REVIEW

2.1 Introduction to neutronics in nuclear reactors

Understanding the background of neutronics is important because it enables a basic understanding of reactor operation. This section provides an overview of the principles of neutronics.

2.1.1 Basic background of ignited neutronics in nuclear reactors

According to Cea (2015) James Chadwick was the first to identify the neutron in 1932 by observing the release of radiation through a chain reaction. Furthermore, Cea (2015) mentioned how neutrons could be used to fission heavy mass isotopes and how such reactions could have led to the meaningful use of power production in nuclear reactors. However, for control and operation, Cea (2015) briefly discussed the characterisation of neutron behaviour in the nuclear reactor, which was referred to as neutronics. In addition Cea (2015) claims that James Chadwick's discovery of the neutron was groundbreaking, as it paved the way for neutronic studies and they point out how neutronics is considered a discipline that is 'seen as a science of microscope.'

2.1.2 The evolution of neutronic studies

According to Lomonosov & Rosatom (2021) the evolving nature of the energy market in regulatory research has led to the high demand for developing neutronic tools for small modular reactor designs. This demand came from the significant difference between conventional designs and the safety regulations of the SMRs, which brought light to the evolution of neutronics.

Many studies have contributed to the development of neutronics by focussing on neutron transport in nuclear reactors, from the early studies to modern studies.

The evolution of the first neutronic studies is mentioned by Nagaya (2025), by touching on the development of the Monte Carlo code MVP for neutron and photon transport calculations since the late 1980s. Nagaya (2025) mentioned the first version of the code, to the newest versions of the Monte Carlo solver Solomon. In the new versions, Nagaya (2025) highlighted the modifications that were made using advanced Monte Carlo methodology for reactor physics applications. In addition, Nagaya (2025) presented recent applications of the MVP code and the Solomon solver to solve eigenvalue and fixed-source calculations for neutron, photon, and neutron-photon coupled transport. In summary Nagaya (2025) clarified the flexibility of MVP codes to solve time-dependent problems, such as neutron noise simulation and pulsed neutron simulation.

Long before studies like Nagaya (2025) existed, was a study that focused on how neutron transport has evolved into dynamic fields such as the medical field (Vaz, 2009). Vaz (2009) managed to portray the evolution of neutron transport to medical fields by emphasising the importance of simulating the criticality of the model, power distribution, activation scattering, and shielding performance for all traditional and emerging technologies. In addition, Vaz. (2009) implemented the Monte Carlo and deterministic radiation transport codes for accurate neutron transport calculations to improve safety, detailed thermo-hydraulics, and radiation damage studies.

A year prior to the publishing of Nagaya (2025) there was literature that claimed that the neutron interaction mechanism was not incorporated truthfully which resulted in the use of a model that involved randomness, such as the stochastic model, to study how particles behaved in a nuclear reactor over time (Melikkendli & Tombakoglu, 2024). That approach by Melikkendli & Tombakoglu (2024) was the introduction of non-analogue stochastic models to study the random behaviour of neutrons and other particles in the reactor.

In the three studies mentioned above, it is evident how the advancement of neutronics has been facilitated in the early to modern commercial reactors. The advancement of neutronics has reached its peak with computational neutronics such as the one found in this study which has expanded to medical fields.

It can be said that the direct advancements of neutronics were initiated by breakthroughs with high impact and theory development. The evolution of nuclear science began with Chadwick's discovery of neutrons and his mastery of the neutron chain reaction. This shows how historical trends amplify financial investments because now it fuels computer technologies and reactor safety.

2.2 Computational neutronic models

2.2.1 Fundamental neutronic codes and methods tailored for different reactor types

To understand the behaviour of neutrons in various reactor designs, several fundamental concepts and introductory mathematical concepts have been established in Lamarsh & Baratta (2014), which revealed the importance of gaining insight into neutron distributions and highlighted the challenges. However, many studies have investigated neutron distributions using mathematical and computational neutronic models on different reactor designs.

2.2.1.1 Pressurised Water Reactors (PWR)

For PWRs, there exist numerous mathematical and computational neutronic models that provided insight on the distribution of neutrons, these include studies that discussed the Nodal Diffusion Theory (Jaradat *et al.*, 2014), Finite Difference Method (Kim & Kim, 2020), Monte Carlo N-Particle Transport Code (MCNP) (Lee *et al.*, 2020), Coupled Neutronic-Thermal-Hydraulic Codes (Ye *et al.*, 2020), and Advanced Codes for Core Analysis (Huda *et al.*, 2011).

2.2.1.2 Boiling Water Reactors (BWR)

The studies that gave insight into computational and mathematical models for BWRs are studies such as (Fridman *et al.*, 2013), which focused on the Nodal Diffusion Theory, while studies by (Kurosawa, 2005) and (Dokhane *et al.*, 2006) focused on Computerised Analysis of Reactor Sensitivity to Monitoring Signals, and Coupled Neutronic-Thermal-Hydraulic Codes, respectively.

2.2.1.3 High Temperature Gas Cooled Reactors (HTGR)

For HTGRs, some studies also touched on MCNP (Leppänen & Dehart, 2009), Finite Element Method (FEM) (de la Torre et al., 2023), Diffusion Theory Approximations (Rohde et al., 2012), Multiphysics Codes (Lemaire et al., 2017), and Simplified Transport Models (Seubert et al., 2012).

2.2.1.4 Fast Breeder Reactors (FBR)

Lastly, studies on FBRs that touch on Monte Carlo N-Particle Transport Codes (MCNP) (Ziver et al., 2004), Finite Difference Method (Vaidyanathan et al., 2010), Finite Element Method (Chellapandi et al., 2007), and Coupled Neutronic-Thermal-Hydraulic Codes (Bonifetto et al., 2013).

There exist assorted types of reactors and more studies, even on the reactors that are mentioned above regarding mathematical and computational models that provide insight into neutron distributions. This section was a brief introduction and overview of extensive research that has been done on exploring neutron distributions.

2.2.2 Neutronic models for high-temperature gas-cooled reactors

In the previous section, a list of different neutronic codes, methods, and mathematical concepts was shown. This section will prioritise neutronic codes that have been used in High-temperature Gas-Cooled Reactors, which will be beneficial for this study. A brief discussion of the codes will be presented along with the literature that has made use of these codes.

2.2.2.1 Serpent

The Valtion Teknillinen Tutkimuskeskus (VTT) Technical Research Centre of Finland has developed the Serpent Monte Carlo reactor physics and burnup code since 2004 (Leppänen & Dehart, 2009). Leppänen & Dehart (2009) additionally highlighted that the code had more than 250 users at that time in multiple organisations for applications that include researching modelling and coupled multiphysics calculations. According to VTT(2022), it was notified that the user statistics are no longer actively maintained, but by 2020 the Serpent community had grown to more than 1000 users in 250 universities and research organisations in 44 countries around the world.

The study by Bostelmann et al. (2016), is one of the studies that has made use of the Serpent code, particularly for the MHTGR-350. Bostelmann's et al. (2016) focused on the comparison of KENO and Serpent results. Although their study focuses on different cross-sections, the main objective of including her work is to see the reactivity difference between the KENO and Serpent results to help with the verification and validation of this study.

2.2.2.2 KENO-VI

The user manual by Wieselquist & Lefebvre (2023) characterised SCALE as a comprehensive modelling and simulation suite for nuclear safety analysis and reactor design development. The manual stated that SCALE was released in 1980, and that the system remained the same even after evolving.

On the other hand, Ilas et al. (2012) helped identify the issues that were faced when modelling the physics of HTGRs. Therefore, it served as a guide in this study to understand and quantify the effect of modelling assumptions on calculations to experiment comparisons.

2.2.2.3 North-West University Reactor Code Suites (NWURCS)

NWURCS is a tool that is used at the North-West University for the analysis of neutronics in many dissertations Nyalunga (2016). The exact term used by Nyalunga (2016) to describe NWURCS is 'Code wrapper'. In addition, Nyalunga (2016) clarified that NWURCS was developed to generate input files for simulation software such as KENO-VI, Serpent, and many more. This simulation software as explained in Nyalunga (2016), are codes used to analyse the behaviour of nuclear reactor cores and may be used to facilitate precise simulation models based on neutron transport theory.

On the other hand, Ringane (2022) focused on the development of a lattice-to-nodal diffusion calculation using a T-NEWT/NESTLE model for the North-Anna (NA) Unit 1 Pressurised Water Reactor (PWR). The important aspect of the study mentioned is the approach to verifying NWURCS. Ringane (2022) used the comparison of the manual calculations of the user with those computed by NWURCS. In addition, Ringane (2022) assessed the accuracy of the NWURCS model by comparing the input and output files generated manually from T-NEWT with the corresponding files from NWURCS. These are the kinds of techniques that were adopted in the verification of NWURCS for the MHTGR-350.

While the study by Nyalunga (2016) provided a clear description of NWURCS, Ringane (2022) helped guide how to approach the verification of NWURCS.

Numerous other studies at the university have used NWURCS for simulations. Although these studies do not focus on the MHTGR-350, their techniques and definitions when it comes to NWURCS were used in this study.

2.3 Fundamental principles for neutronic analysis

According to Zahuri et al. (2018) neutronic behaviour is painted as an important aspect when it comes to analysing nuclear reactors, providing accuracy in the performance, safety, and optimisation of the reactor design. A list of techniques to use for the analysis along with reasons why they are used are explained in this section; however, the focus was on three techniques that will be of use later in this dissertation.

Some papers such as Fortini et al. (2015), focused on SCALE models for fuel cycles and reprocessed fuels, and others such as Nyalunga (2016) focused on neutronics. In the reactor analysis research group at the NWU, there is a gap in the research because there is no focus on the safety parameter calculations to assist with regulatory applications. This resulted in the aim of this study to focus on calculating safety parameters for regulatory research.

2.3.1 The Analogue Method of Monte Carlo

The analogue method for Monte-Carlo, as mentioned in Section 2.2, is a method that was established to truly incorporate the interaction of neutrons by studying how particles behave in a reactor over a certain time. In Gordon et al. (2021), this method is used to model the stochastic behaviour of neutrons in fixed neutron source applications. The study clarifies that the accuracy of this method strongly integrates with the computational efficiency of the mathematical models they used. This study uses the KENO-VI code to develop a model that will be used for neutronic calculations, and according to Wieselquist & Lefebvre (2023), KENO-VI uses Monte-Carlo methods for criticality calculations.

2.3.2 Source convergence

Cheng et al. (2024) explains source convergence in the context of Monte Carlo criticality calculations, stating that it is an iteration process of stabilising the fission source distribution, and if it is not diagnosed properly, it could potentially lead to inaccurate k_{eff} results. In addition, Cheng et al. (2024) reported on the improvement of the calculations for loosely coupled systems by making use of the distribution of fission sources. That enhanced version was said to be able to accurately determine the convergence within a system made up of complex geometries.

2.3.3 Theory and the Application of Tallies

Ibrahim et al. (2010) gave a brief explanation of how tallies are a representation of the quantities calculated during simulations; those quantities included the particle flux, reaction rates, and energy deposition.

Ibrahim et al. (2010) further elaborated on the uses of tallies, how they are used to evaluate neutron and gamma flux distribution across reactor geometries, how they are used in the calculation of specific quantities such as radiation doses outside shielding, and finally how they are used to serve as metrics for the optimisation of reactor design.

This study will use these elaborations to execute the objectives of the paper but for the distribution of flux across the International Thermonuclear Experimental Reactor (ITER) and also includes forward weighted continuous adjoint importance sampling to improve the accuracy of the tally calculations. Although great progress has been made in modelling and simulating complex geometries such as the ITER (Ibrahim et al., 2010), one concern is whether the same accuracy can be obtained when dealing with geometries such as the MHTGR-350. This research will address the limitation by using tallies to represent neutron flux.

2.4 Introduction to the reactor details of the MHTGR-350

In Chapter 1, a basic introduction to the layout of the MHTGR-350 is provided. To expand the understanding of the reactor that is analysed in this dissertation, more information such as features, characteristics, and design needs to be discussed, starting with the basic background of the MHTGR-350.

The existence of the MHTGR-350 design, according to Ortensi et al. (2015) has been around for more than 40 years. The design is characterised by the inclusion of its advanced safety features, such as managing decay heat removal without the intervention of the operator, and the ability for heat to dissipate via the reactor cavity cooling system, which operates through natural air circulation. In addition to safety features, the incorporation of the helically coiled steam generator within a dedicated vessel and the well-established technology used for the steel is also included (Ortensi et al. 2015).

Researchers do not necessarily create or design reactors from scratch; instead, a development of models from data obtained from trusted sources such as the IAEA and Ortensi et al. (2015) is carried out along with an analysis of such models to meet the objectives of their work. Using this perspective, the reactor specifications used in this dissertation were extracted from Ortensi et al., 2015).

This section focuses on the design and implications of the MHTGR-350 and will also provide the specifications of the exact reactor design that will be used to carry out the objectives of this dissertation by comparing them to the specifications from Ortensi et al. (2015).

2.4.1 Coated Fuel Particle Design

The most well-known safety feature in the HTR Generation-IV reactor is the design of the fuel component; this section aimed to explore the intricacies of the fuel component of the MHTGR-350.

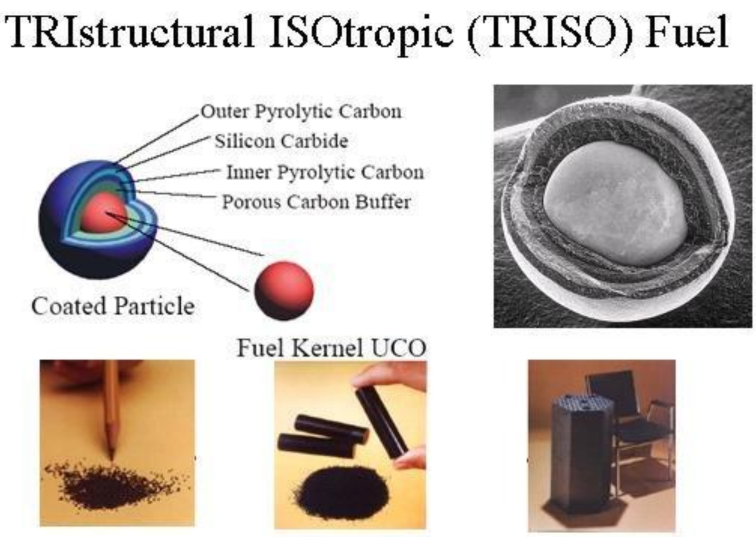

Figure 2-1: Triso fuel-coated particle (Laranjo De Stefani, 2017)**.**

As seen in Figure 2-1, the spherical fuel particle commonly known as the TRISO fuel particle has layers of coating surrounding the fuel kernel where $U0_2$ or UCO reside. These four layers of coatings fulfil distinct roles, and those roles as seen in Wells BE et al. (2021) as given next.

The buffer: The buffer creates a space for the accumulation of fission gas and accommodates the recoils caused by the fission. It mechanically decouples the kernel from the inner pyrolytic carbon (IPyC) layer, accommodating any kernel swelling during operation.

Inner Pyrolitic Carbon: It protects the kernel from corrosive gases during SiC deposition and contributes to the retention of fission gases.

Silicon carbon: Its purpose is to retain non-gas fission products and maintain pressure within the particle during operation.

Outer Pyrolitic Carbon: It adds to the gas retention and protects the SiC layer as well as being a bonding surface.

The fuel element description in this study is consistent with those found in Ortensi et al. (2015).

2.4.2 Fuel-Compact Design

These TRISO-coated particles as seen in Figure 2-2 were embedded in a graphite matrix to enhance the heat transfer and moderation of neutrons that exit the TRISO-coated particle (Wells et al., 2021). These TRISO-coated particles were embedded in the graphite matrix to form a fuel compact/fuel pellet. Similarly to a fuel compact, there is a burnable poison compact.

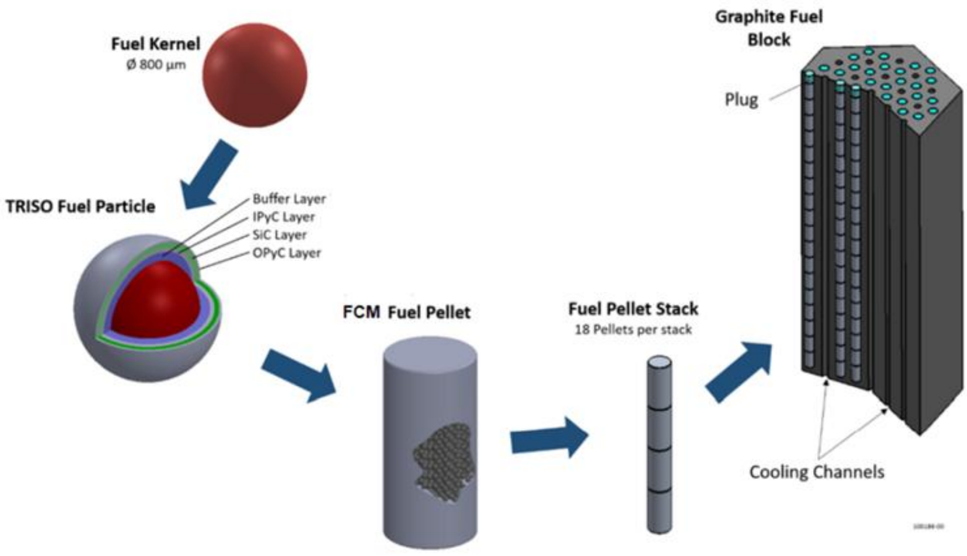

Figure 2-2: Overview of the TRISO compact fuel concept (Schappel et al., 2019)**.**

2.4.3 Hexagonal fuel and reflector blocks

The TRISO-coated particles which were embedded in the graphite matrix to form fuel compacts, were stacked on top of each other and form 'fuel rods' as mentioned in the previous sub-section and shown in Figure 2-2. These fuel rods were then placed in cylindrical holes as stated in Aihara et al. (2014), to form a fuel block. The hexagonal fuel block is the equivalent of the PWR fuel assembly. Figures 2-3 and 2-4 show a clear overview of how a fuel block is created as described in this section.

There are 210 fuel compacts per block, 102 large coolant channels, and 6 small coolant channels. The homogenised burnable poison compact was placed in 6 blind holes.

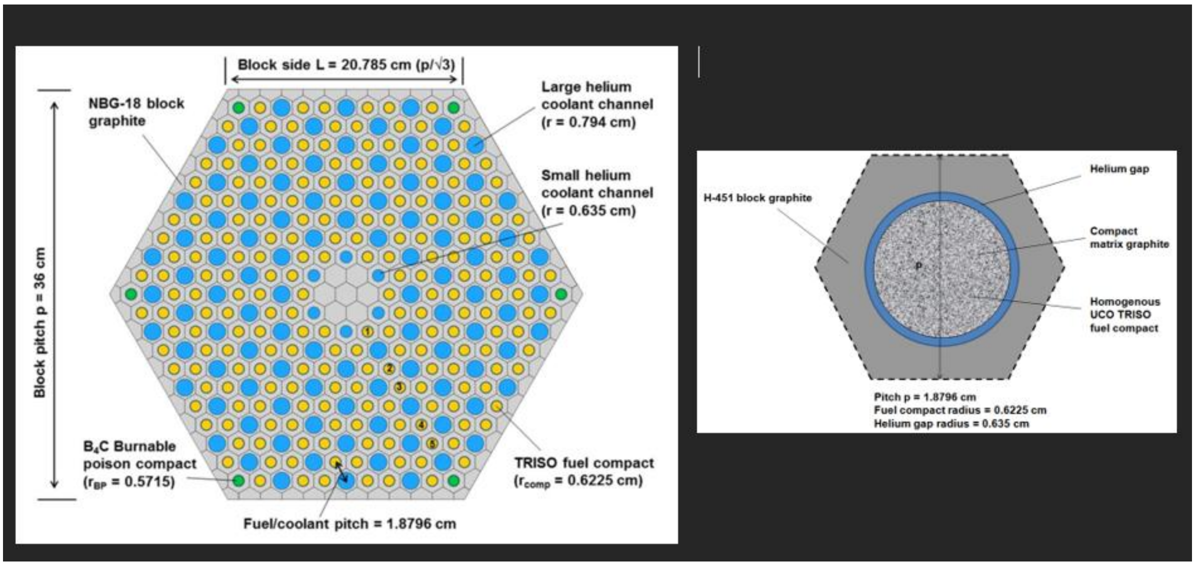

Figure 2-3: Hexagonal fuel blocks and close-up of the fuel pitch (Strydom, 2020)**.**

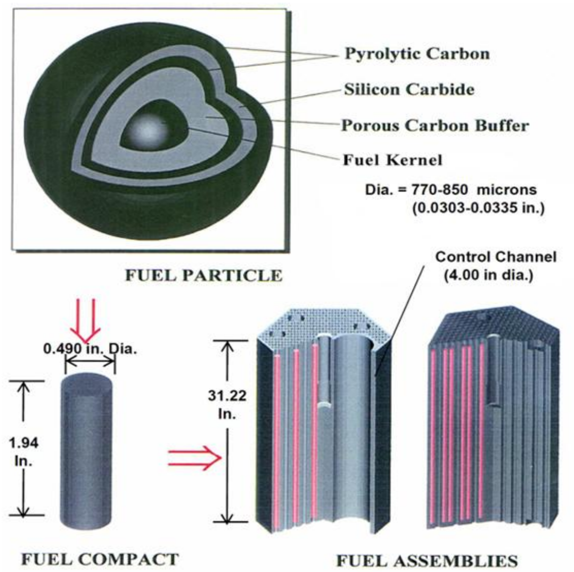

Figure 2-4: Overview of how a fuel block is created (Benson, 2022).

2.4.4 Full core configuration

The MHTGR-350 configuration is an annular core composed of hexagonal fuel blocks, hexagonal reflectors, and control rod channels, as seen in Figure 2-5. The full core was designed to have inner hexagonal graphite blocks in the centre. Some of these have control rod holes. The hexagonal fuel blocks surround the inner blocks, some of which also have control rod holes. Finally, the fuel blocks are surrounded by hexagonal outer reflectors, some of which also have control rod holes. This configuration of the arrangement of hexagonal inner blocks, fuel blocks, and outer reflectors was arranged to create a hexagonal shape. Figure 2-5 shows a top and side view of the annular core for the MHTGR-350 (Wang et al., 2020).

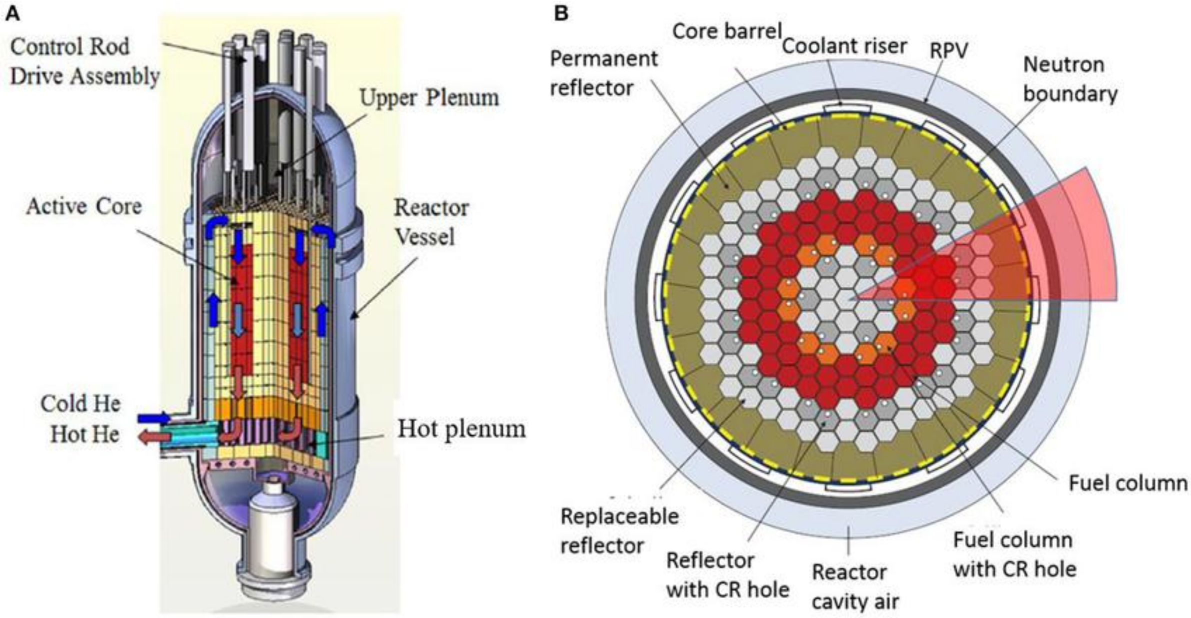

Figure 2-5: MHTGR design: (A) cutaway view of the RPV and (B) cross-sectional view of the reactor core (Wang et al., 2020)**.**

The helium coolant flows in the direction starting from the upper plenum and exits in the lower outlet plenum (Lemaire et al., 2017). Lemaire further explained that a fraction of the core flow bypassed the fuel block coolant holes and passed through the hexagonal gaps, as seen in Figure 2-5 and the cooling channels of the control rod.

The coated particles per core was the only design parameter that needed to be calculated, and this was done by calculating the number of compacts per channel in a block, then multiplying by the channels per block and then by the total number of blocks. Note that because of the control rod holes, the number of channels per block were different.

2.4.5 Operating Characteristics of the Reactor

The tabulated overview of the reactor is provided below; these tables present the key specifications, including structural configurations, operational limits, and essential parameters that define reactor performance (Ortensi et al., 2015).

Table 2-1: Design and Operating Characteristics.

MHTGR-350 Characteristics	**Value**	**Value from** Ortensi et al. (2015)
Reactor Power	300 $MW(t)$	350 $MW(t)$
Installed electric capacity	141.428 $MW(e)$	165 $MW(e)$
Fuel	Prismatic Hex-Block fuelled with Uranium Oxycarbide fuel compact of 15.5 wt% enriched U-235 (average)	Prismatic Hex-Block fuelled with Uranium Oxycarbide fuel compact of 15.5 wt% enriched U-235 (average)
Primary Coolant	Helium	Helium
Primary coolant pressure	2.400E+05 Pa	6.39 MPa
Moderator	Graphite	Graphite
Core outlet temperature	650 K	960 K
Core inlet temperature	300 K	532 K
Mass Flow Rate	171.00 kg/s	157.1 kg/s
Reactor Vessel Height	9.9126 m	22 m
Reflector DIAM	3.173 m	6.8 m

Table 2-1 showed a noticeable difference regarding the first characteristic, highlighting a key distinction between the two datasets. The power of the modelled MHTGR-350 was made to be 300 $MW(t)$, while the reference model was taken to be 350 $MW(t)$, it is important to note that using models with predefined reactor parameters allows for consistency between this model and the already validated data; however, such adjustments were not foreign in the world of research. Although this difference did not weigh on the outcome of this study, this discrepancy needs to be adjusted so that future studies exploring the model used in this dissertation correspond to the Ortensi et al. (2015) benchmark model.

Due to the interconnection between the electrical power and the power of a reactor, an increase in power will increase the electrical capacity of the reactor.

Another discrepancy was observed in the primary coolant pressure of $2.400E + 05\ Pa$ and that of Ortensi et al. (2015) given as $6.39\ MPa$, which also did not affect the outcome of the neutronic study.

Another noticeable difference between the two models was the inlet and outlet temperatures, which appeared to be lower than those of the ones given in Ortensi et al. (2015). The reason for this was that, the model used in this dissertation gave a clear representation of the isothermal cold case as a start-up state; this along with the reasons for the discrepancies mentioned above are explained in the verification of the Serpent base model in Chapter 4.

The mass flow rate as explained in Chapter 4 was used to calculate the axial temperature difference of the core and, similarly to the power, it did not affect the outcome of this dissertation because it dealt with thermal and not neutronic calculations. Furthermore, the base model of this study was the isothermal case, as mentioned above.

A neutronic model needed to be spatially bounded because the larger the model, the more expensive it got to get the value of k_{eff}, this was the reason for the difference in the core height of this model and the other. Calculations were done to check the effect size had on k_{eff} and it was proven that it took more time to run the model when the height is larger, the results were be seen in Chapter 4.

2.4.6 Safety report on the MHTGR-350

It is obvious from the introduction that safety in nuclear reactors remains important considering the potential risks associated with nuclear energy. The safety of the employees was ensured by taking all possible precautions to protect individuals, the environment, and the facility from exposure to radiation or accidents that cause a malfunction. In nuclear reactor physics, the temperature coefficient is considered an important parameter due to how it defines the reactivity of the reaction of a reactor to different temperatures (Lamarsh & Baratta, 2014).

The ways in which safety can be implemented were extracted from the report Slbady & Millunzi (2007), which focussed on a detailed analysis of the design of the MHTGR-350 and its safety features. The report provided four in-depth user requirements to produce a safe and economical power plant, which are maintaining a safe plant operation, maintenance of plant protection, maintaining control of radionuclide release, and maintaining emergency preparedness.

However, the IAEA provided a more detailed report in IAEA (2010) on the safety of the MHTGR, by directing their focus on accident analysis. The IAEA (2010) addressed events that may lead to fuel failure and subsequent radioactivity release, which is similar to SIbady & Millunzi (2007). Although safety reports are somewhat similar, the report done by IAEA (2010) has a different methodology. It grouped accidents according to their probability of occurrence and provided guidance on how to analyse the situation.

The two reports were highly beneficial to this study, as they incorporated model validation, design criteria, and safety mechanisms into the model, and provided insight into reactor physics and emergency preparedness. However, both studies were more theoretical in their approach. Therefore, this dissertation adopted a more quantitative (computational) approach by considering both computational and theoretical calculations, keeping both reports in mind.

2.4.7 Licensing and Reactor Certifications

The nuclear reactor licencing remains another important aspect. It is there to ensure that nuclear reactors meet the safety standards through an assessment of the design and operation before deployment.

The steps to licence a nuclear reactor as mentioned in Safety Guide Report IAEA (2010) include the first step, which is a pre-application; this consists of the applicant having early discussions with the licencing authority to clarify the requirements and expectations of the licence application. This step is followed by the actual application, where the application is prepared and submitted to the authority with detailed safety documentation, including environmental and safety analyses, technical specifications, and design information on the nuclear plant in question. Then the authority reviews the documents presented with due regard to their suitability with the safety standards and other regulatory requirements. This then licences the operation, with a few stipulations to ensure safety. Proceeding is the construction and commissioning begin where the regulatory body monitors construction and commissioning further into the nuclear installation, to ensure that all safety needs have been considered. The second last step is the operation licence; This is the part where the operational licence issued after successful commissioning allows the nuclear installation to enter its operational life under supervision. Finally, the decommissioning, this last step at the end of the operational life of a nuclear installation, makes sure that the procedures for disposing radioactive materials is followed and established in a safe way.

Nuclear reactor licences may differ depending on the country. The IAEA licencing process is indispensable as it ensures necessary safety measures, starting from design up to accident analysis to measure up to international standards. In conclusion, the report guide focusses on how to identify the model by detailing the requirements for accident scenarios and risk-informed decisions, so that the report can be more robust and consistent with real regulatory practice.

2.4.8 Reactivity Coefficients

2.4.8.1 Temperature coefficient

In nuclear reactor physics, the temperature coefficient remains an important parameter due to how it defines the reactivity of the reaction of a reactor to different temperatures. It was mathematically described by determining how neutron interactions with materials change as the temperature varies. Specifically represented mathematically in Alhassan et al. (2010) as follows:

$$\propto_{\boldsymbol{T}} = \frac{\boldsymbol{d\rho}}{\boldsymbol{dT}} \qquad 2\text{-}1$$

Where $d\rho$ is the change in reactivity and dT is the change in temperature of the materials in consideration.

The equation defines the change in reactivity by changing temperature, and a negative coefficient will be better for reactor stability, since it helps to prevent overheating and keeps the plant safe. The knowledge of this coefficient and its calculation is very important in the proper development and operation of reactors, especially in the balance of thermal neutrons and fast neutrons between different types of reactors (Lamarsh & Baratta, 2014).

2.4.8.2 Fuel temperature coefficient

According to the educational part of reactor physics and kinetics published by the International Atomic Energy Agency, the fuel temperature coefficient is the reactivity change due to one unit of change in the temperature of the fuel. They continue to say that in an operating reactor, temperature changes are proportional to power changes. When the power increases, the number of fission reactions that occur also increases; thus creating more heat which results in a rise in the reactor core temperature (Lamarsh & Baratta, 2014).

The equation used to calculate the fuel temperature coefficient is provided by the IAEA and Nuclear Reactor Physics (2005) as follows:

$$\propto_{fuel} = \frac{d\rho_{fuel}}{dT_{fuel}} \qquad 2\text{-}2$$

Where, $d\rho_{fuel}$ is the change in reactivity of materials that consists of the fuel and dT_{fuel} is the change in temperature of all materials that consist of the fuel.

Talamo (2007) focused on the result of changing the fuel temperature reactivity coefficient for the pebble bed and the prismatic high temperature reactor. They made use of two different fuels, and the result was that increasing the temperature of the fuel increases the Doppler broadening of the resonances in the fuel nuclides.

2.4.8.3 Moderator temperature coefficient (MTC)

Mourtzanos et al. (2001) focussed a lot on the MTC theory and explains it well, since it remains an important operational variable of reactors. He defined the MTC as the reactivity change that corresponded to a one-degree increase in the core-averaged moderator temperature. In addition, Mourtzanos et al. (2001) specified how it is common practice to design the reactor core to have a negative MTC to guarantee negative reactivity feedback in the event of a power excursion depending on the reactor design during power excursions, such as during the change in reactivity. Although Mourtzanos et al. (2001) focussed on PWRs, the definition and importance of the MTC applied to high-temperature gas-cooled reactors (HTGRs), and the key differences between the two reactor types, should be considered in the calculations.

Using the general theory of Alhassan et al. (2010), the equation used to calculate the MTC is provided by:

$$\propto_{\mathrm{moderator}} = \frac{\mathrm{d}\rho_{\mathrm{moderator}}}{\mathrm{dT}_{\mathrm{moderator}}} \qquad 2\text{-}3$$

Where $\mathrm{d}\rho_{\mathrm{moderator}}$ is the change in reactivity of the moderator and $\mathrm{dT}_{\mathrm{moderator}}$ the change in temperature of the moderator.

2.4.8.4 Neutron flux

Lamarsh & Baratta. (2014) gave a clear explanation of neutron flux and helped visualise it as the number of neutrons in a reactor core that strike a unit target area at different energies simultaneously. Additionally, they displayed the equation used to define the neutron flux, written as:

$$\emptyset = \boldsymbol{nv} \qquad \text{2-4}$$

Where n is the intensity at which the neutron strikes the unit area and v is the velocity of the neutron.

2.4.9 Summary

This chapter used the funnel method to discuss literatures that was beneficial for this study, starting with the background of neutronics that assisted in understanding the neutronic models, which were discussed next followed by the discussion of the MHTGR-350. The features and characteristics of the MHTGR-350 were explored. The chapter concluded with the discussion of the reactivity coefficients.

CHAPTER 3 METHODOLOGY

3.1 Overview

The primary focus of this chapter is to provide the methodology used to achieve the objectives of the research study and how the development of the neutronic model came about.

The core aspect is to provide a detailed analysis of the measures that were taken to identify the safety parameters, the calculation of the parameters, and the development of the base model using NWURCS as the base input for both the Serpent and KENO-VI/SCALE codes. Additionally, an outline of the steps that were taken to verify the model will be discussed, along with how the comparative analysis with other HTGRs and LWRs was done, and, in conclusion, how the results were interpreted in the larger context of the reactor.

3.2 Research approach and design

90% of this study made use of the quantitative approach with the remaining 10% utilising the qualitative approach. The 10% qualitative approach included the experiences regarding nuclear accidents, but overall the quantitative approach was used in the implementation of computational and software resources to calculate, collect, and analyse results.

With regards to the literature review, the comprehensive funnel method of existing literature was used to provide a solid foundation for the study. Key references include seminal works and recent advancements in the field, ensuring a well-rounded understanding of the subject matter.

Finally, the verification of the model using Excel and Word was implemented, and all the data was stored in their respective files in the C drive and backed up using an external source.

3.3 Reactor type selection

To conduct a study on a small modular reactor an existing model was made available, due to the scope and limitations of a masters research project, which thus formed the basis of this study. Before any calculations were made, the model was verified and validated for applicability and accuracy.

The pebble-bed-type reactor would be the reactor of choice given the history of the Pebble-Bed Modular Reactor (PBMR) in South Africa. However, it is also wise to consider a prismatic reactor given the more stable core configuration in terms of the position of the fuel elements. In the pebble-bed reactor, the pebbles are continuously moving, whereas in the prismatic reactor, the prism block is stationary and is only changed in position or removed from the core during reload. The HTGR prismatic reactor is part of the growing interest in Small Modular Reactors (SMRs) worldwide, it has several key advantages in the context of South Africa by contributing to the nation's energy diversification with a reliable low carbon baseload source of energy, considering that South Africa is highly dependent on coal and intermittent renewables. The MHTGR-350, if chosen, will provide stability to the energy grid of the country, thus ensuring continuity in the generation of power with reduced GHG emissions.

Thoughts were expressed on how the modular nature of this device could make deployment possible in remote areas; this is a factor that is suitable for South African power needs.

More insights are given into the most crucial and positive feature of the MHTGR-350, which is the safety aspect; there are passive safety features designed particularly for the HTGRs, which are discussed in Chapter 2. The MHTGR-350 is a type of reactor that is part of an international effort to build smaller, more flexible nuclear plants that are cost-effective and scalable.

This resulted in a deeper understanding of how the high temperature operability of the MHTGR-350 would contribute to making it highly efficient for more uses, including hydrogen production. Furthermore, the high fuel efficiency and reduced production of radioactive waste from the reactor would be enough to meet the country's commitment to sustainability and protection of the environment.

As a result of this understanding, the door will open for more regulatory research on MHTGR-350 to explore the potential of these units being safe and economically viable in the long-term energy supply while contributing internationally to the debate on the deployment of SMRs.

Ultimately, the insights gained highlight the importance of the MHTGR-350 or any small modular HTGR for regulatory studies.

3.4 Reactor Setup

3.4.1 Level Layout

NWURCS uses the concept of levels to refer to regions within a core where materials and many more elements are placed. This is quite useful in reactors such as this one and other advanced reactors due to the layers and segments, where different regions within the core exist for fuel, moderators, reflectors, and control rods. The model of this dissertation consists of a four-level structured reactor and to help with understanding the reactor, levels are introduced, along with their graphical representation. To facilitate the discussion, level 4 is first discussed, followed by level 3, 2, and finally level 1.

- Level 4: Level four consists of the coated fuel particle that has four coated layers and, as seen in Table 2-1 every coat has a radius of not more than $0.05\ cm$. This emphasises how tiny the fuel particle is. Below is an image of the coated particle as seen in the reactor.

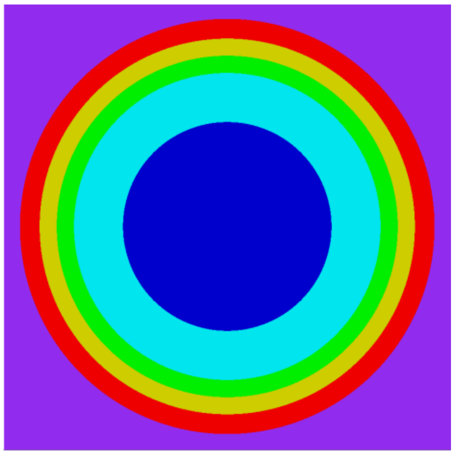

Figure 3-1: Top view of fuel compact with fuel particle inside.

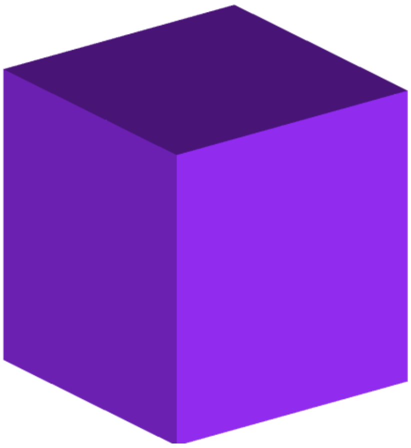

Figure 3-2: 3D Isometric view of the fuel compact.

Level 3: This level consists of coated particles that are placed in fuel compacts; the figure below illustrates how the coated particles are placed or packed in fuel compacts. Fifteen of the fuel compacts are stacked on top of each other to make up a “fuel rod”, therefore, in one “fuel rod” there are 15 fuel compacts. For the current model, the TRISO particles are placed in a structured cubic lattice in the compact. In reality, the TRISO particles are placed randomly in the compact. Serpent has the capability of placing the TRISO particles randomly in the compact, implicitly done using code algorithms. However, KENO-VI would require explicit modelling of the position of the TRISO particles in the compact, and this would require huge computer memory for the full core. Therefore it was not pursued here. To allow comparison between Serpent and KENO-VI, the structured cubic lattice was implemented. The use of random particle positions in the compact is necessary for the correct base model. However, due to the time constraints of this study, this

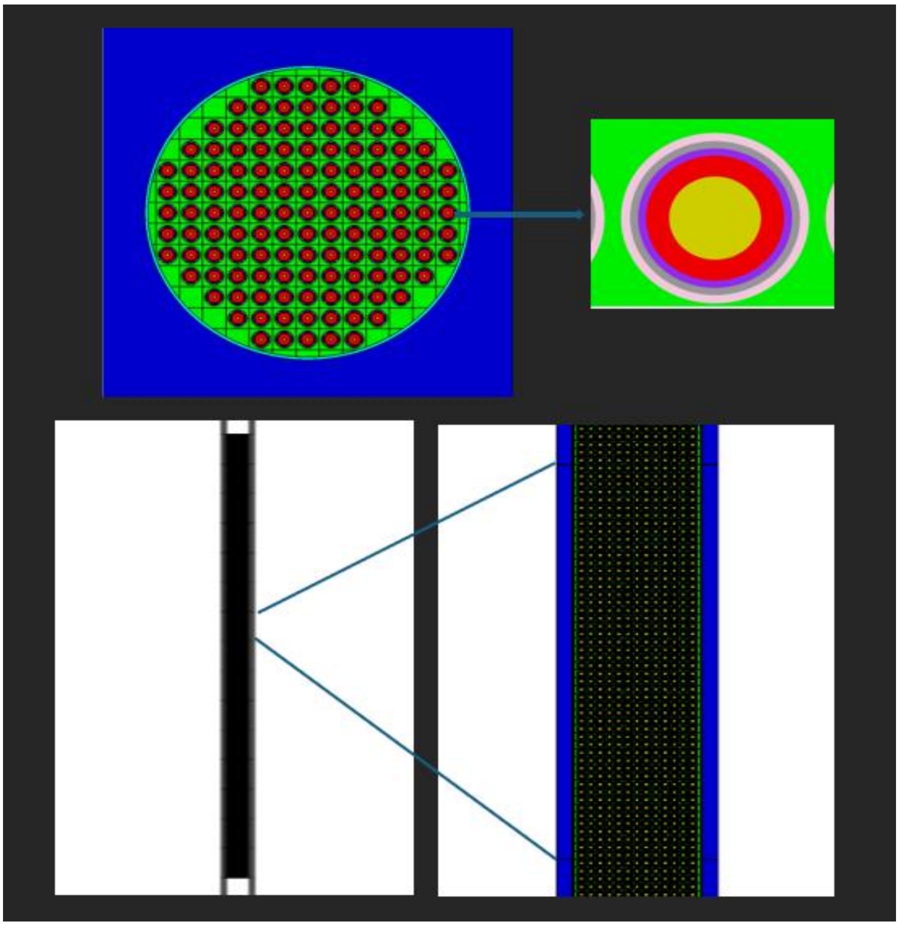

implementation in Serpent is reserved for future work.

Figure 3-3: Top view of the stacked fuel components and 'fuel'.

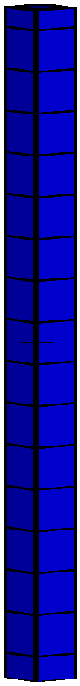

Figure 3-4: 3D view of the "fuel rod".

- Level 2: 108 'fuel rods' are placed in fuel holes in the hexagonal graphite block to make up a fuel block, the images below represent the fuel blocks that are generated from 'fuel rods'.

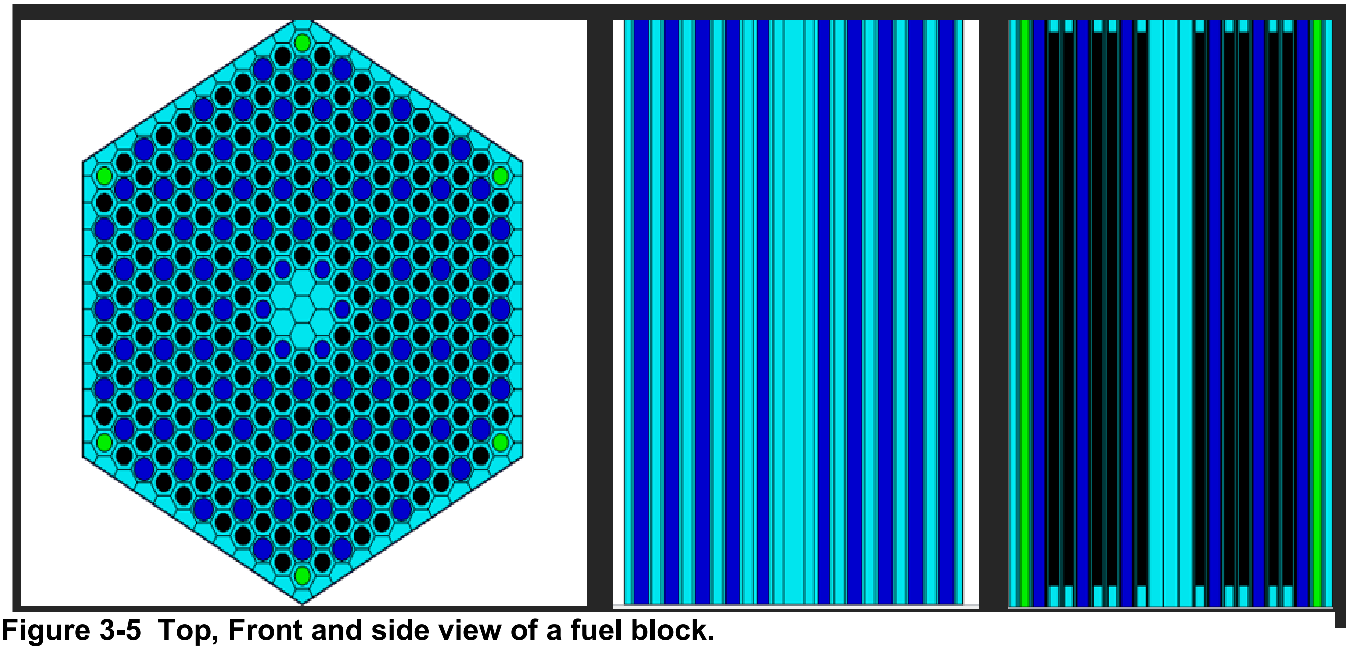

Figure 3-5 Top, Front and side view of a fuel block.

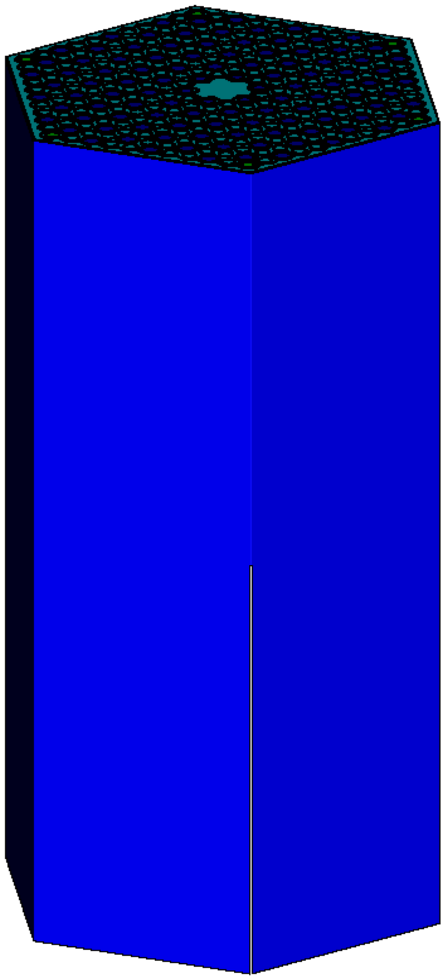

Figure 3-6: 3D isometric view of a fuel block.

Level 1: This is the first level that contains levels 2-4, it is known as the full core. It includes the hexagonal blocks as seen in Figure 3-6, which are the fuel blocks, reflector blocks, and the reactor pressure vessel.

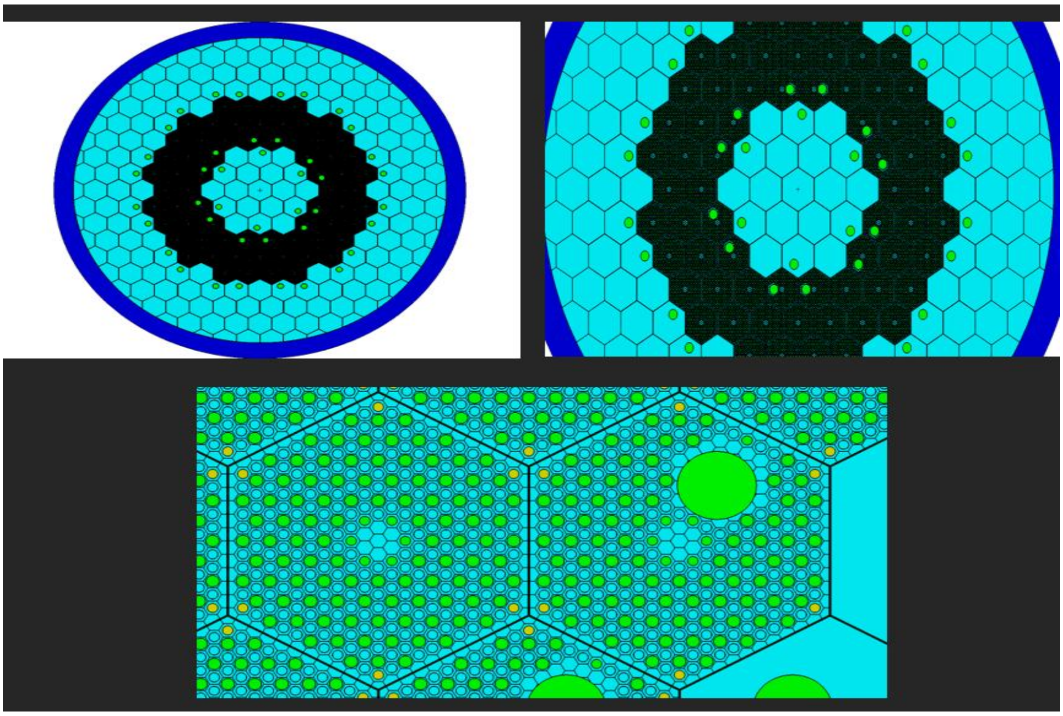

Figure 3-7: Full core top view with close-up view of levels 1,2 and 3.

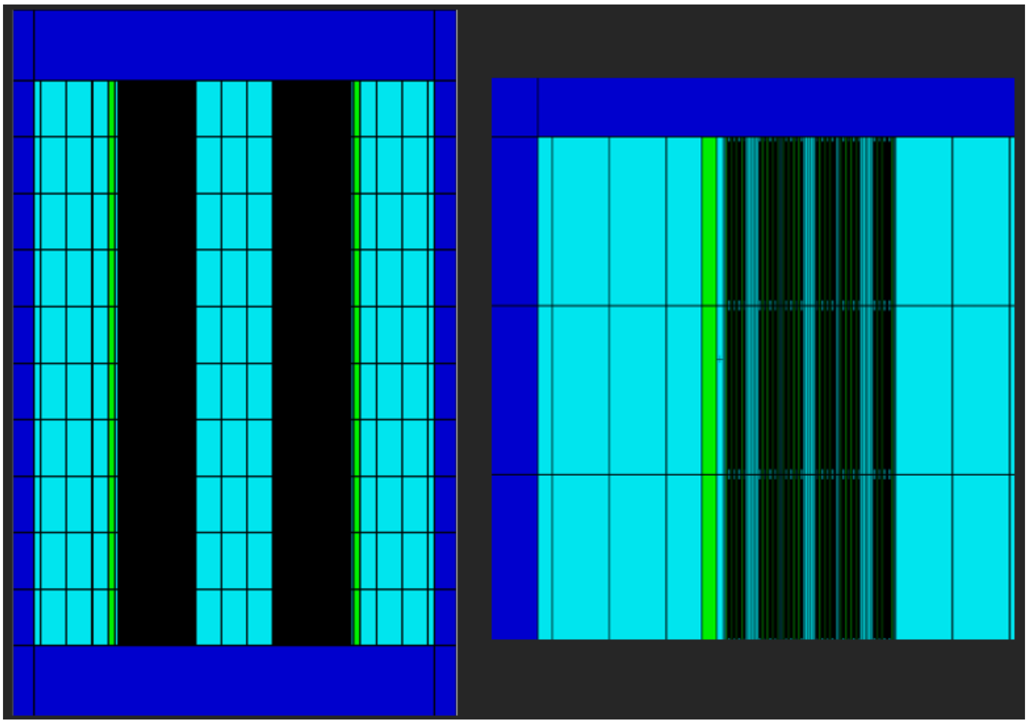

Figure 3-8: side view of the full core model.

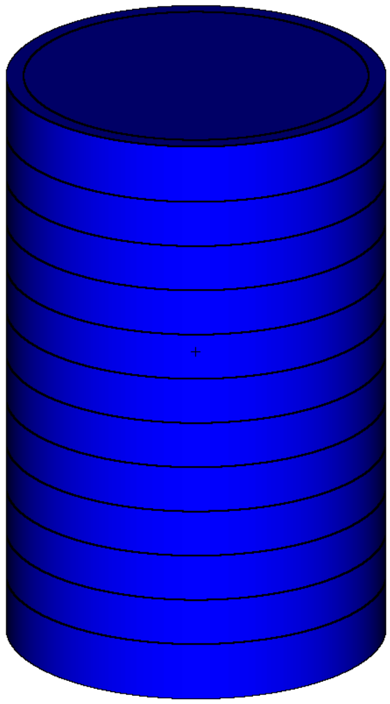

Figure 3-9: 3D view of the full reactor core.

3.5 Neutronic Safety Parameters

3.5.1 Identification of the safety parameters

The selection of the key safety parameters was the challenging part of the research because it was not based on the importance of the safety parameters, but it was based on which topics are very important so that the focus can be on those topics. The parameters included were:

- Moderator temperature coefficient of reactivity, and
- Fuel temperature coefficient of reactivity.

In the process of identifying these parameters, consideration of the aim of this dissertation became the primary point of reflection, as the focus was on parameters that affect neutronics, and it boiled down to the two safety parameters mentioned above, given the time constraint of the project.

3.6 Computational Resources and Software

It is essential to select software that best fits the objective of a study and in this dissertation, the selected software was described to best fit the aim of this study, and a detailed explanation of why and how the selection came about is provided below for each software.

3.6.1 NWURCS

NWURCS was chosen due to its proven accuracy and reliability through its results in many dissertations and research papers produced at the North-West University and its accessibility, these include Nyalunga et al. (2016), Sihlangu et al. (2021), Ringane TP (2022) and many more. It also interfaces well with codes such as KENO-VI and Serpent, which allows comprehensive analysis and enables comparisons to be made.

Furthermore, NWURCS is supported in terms of academia at North-West University, and its past application history in HTGR research, together with cost-effective running within a facility, made it a suitable fit for this project.

NWURCS in this regard was used as the 'code wrapper' to generate input files for the KENO-VI and Serpent software.

3.6.2 Serpent

Serpent is a code designed to produce homogenised multi-group constants for deterministic nodal diffusion codes using continuous-energy Monte Carlo methods for the next-generation reactor system. It has been proven to produce reliable results for the North-West University and worldwide. It has gained wide recognition in the nuclear engineering community by verifying against experimental data and benchmark tests. In this study, the model was extended to model the full core instead of only the fuel assemblies or fuel blocks. The advanced features that were used in this dissertation enabled investigating the influence of several input parameters on the reactor behaviour, and the MHTGR-350 being the next generation of reactors makes the code system suitable for this dissertation. One major limitation as applied by NWURCS is the function of modelling the random distribution of the coated particles. While the commands to be used in Serpent are relatively simple, it needs to be coded in NWURCS.

3.6.3 SCALE 6.2.3/KENO-VI

As defined in Chapter 2, SCALE is a code system designed for nuclear safety analysis and design, it was selected exactly for this purpose, but the most consideration went to the code system that did not have a lot of research being done on the analysis and design of the MHTGR-350.

The features that were received from this software, that were of greater use for this dissertation was the precision in complex geometries. The geometry for the MHTGR-350 is complicated due to its prismatic design and the double heterogeneity of the coated particles in the compact that are not present in the conventional PWRs. The software was able to provide clear and accurate images used to represent the MHTGR-350, which also made the verification process smoother.

Additionally, the comparison of both SCALE\KENO-VI and Serpent models further contributes to the verification of both models, increasing the reliability of both models, given their similar features derived from the common NWURCS base files.

However, as discussed earlier, modelling of the positions of TRISO particles needs to be carried out explicitly, and this would require a lot of memory. Therefore, it was not pursued in this study.

3.7 Source convergence and reduction of the standard deviation

The convergence testing of the neutron population distribution of Serpent and KENO-VI codes is done to ensure reliability in the results. The idea was to increase the inactive or skipped cycles until the neutron source reaches convergence.

In this work, a set of simulations was carried out by gradually increasing the number of inactive cycles from 100 to 1600 in the Serpent code. This was done to establish when source convergence is achieved, i.e. the source is evenly distributed over all fissile sites. This was assessed using the Shannon entropy from the output results.

After source convergence was achieved, active cycles were run and similar to the Shannon entropy; standard deviation and the average of the multiplication factor (k_{eff}) were recorded as provided by the output results of the Serpent code. These factors were tabulated. If the standard deviation was greater than 10 pcm, the number of active cycles would be increased until the desired standard deviation was achieved. This is done to produce results that are reliable and accurate.

As for the KENO-VI code, source convergence is already displayed in the output file, therefore, it will be clear from receiving the results if the source has converged.

For source convergence, a scatter plot graph with straight lines was implemented, where the Shannon entropy results were displayed on the y-axis and the number of total cycles on the x-axis. The inactive cycles are considered to converge when the pattern of the plotted data shows a stabilising/aligning trend.

3.8 Verification of the KENO-VI and Serpent Model

The verification of both models was done to check if the results received corresponded with each other, and upon realising that the results deviated from the expected outcome, the verification of the Serpent model was done using Ortensi et al. (2015). The code verification between the KENO-VI and Serpent output results was done; the results along with the discussions can be seen in the next chapter.

The primary purpose of the KENO-VI code verification was to build confidence in the accuracy and reliability of the results for the calculation and analysis of the safety parameters. The process helped identify errors in the input data, facilitating timely notification of discrepancies that could have resulted in costly mistakes. It also assists the NWURCS code developer in identifying the algorithms that require remediation.

3.8.1 Reducing the level scheme

To investigate where the large difference between the KENO-VI and Serpent codes came from, the models had to be broken down into homogenised levels. This was carried out as follows:

Model at level 1: The reactor core was homogenised to be a single material, UO_2. There were no fuel blocks.

Model at level 2: The reactor core consisted of the fuel blocks, with 10 axial levels (i.e., 10 layers of blocks). However, each fuel-block consisted of a single material, UO_2.

Model at level 3: Using the model at level 2, the heterogeneity of the fuel block is reintroduced. This means that the coolant channels and fuel compacts in the fuel channels in the block were modelled. However, the fuel compacts did not contain the coated particles; instead, they were modelled as a single homogeneous material, UO_2.

Model at level 4: Using the model at level 3, the heterogeneity of the compact was modelled. This means that the coated particles were modelled using a lattice.

3.9 Calculation of the safety parameters and their errors

Equations 2-1, 2-2, and 2-3 were used to calculate the temperature coefficients such as the fuel temperature coefficient and the moderator temperature coefficient.

However, the linearity of the data was first tested. To do this, six data points were chosen, with the corresponding values for the multiplication factor. A linear least square fit was applied to the data, from which the slope would yield the reactivity coefficient. The method for this analysis is given in Taylor (2022) together with the error.

The linear equation can be expressed as follows:

$$\boldsymbol{y = A + Bx} \tag{3-1}$$

Where the coefficients for the linear equation fitted are given by:

$$\boldsymbol{A} = \frac{\sum x^2 \sum y - \sum x \sum xy}{\Delta} \tag{3-2}$$

$$\boldsymbol{B} = \frac{N \sum xy - \sum x \sum y}{\Delta} \tag{3-3}$$

And

$$\Delta = \boldsymbol{N \sum x^2} - (\textstyle\sum \boldsymbol{x})^2 \tag{3-4}$$

With the residual defined using the equation:

$$\boldsymbol{R} = \sqrt{\textstyle\sum (\boldsymbol{Y_c} - \boldsymbol{Y_{LF}})^2} \tag{3-5}$$

Where, Y_C are the calculated values and Y_{LF} are the corresponding linearly fitted values.

With the errors calculated using the following equations:

$$\boldsymbol{\sigma_y} = \sqrt{\frac{1}{N-2} \sum_{i=1}^{N} (y_i - A - Bx_i)^2} \tag{3-6}$$

$$\boldsymbol{\sigma_A} = \boldsymbol{\sigma_y} \sqrt{\frac{\sum x^2}{\Delta}} \tag{3-7}$$

$$\boldsymbol{\sigma_B = \sigma_y \sqrt{\frac{N}{\Delta}}} \quad 3\text{-}8$$

3.10 Neutron flux

To analyse neutron flux, the use of graphs was implemented along with the percentage difference by making use of the following equation.

$$\boldsymbol{PERCENTAGE\ DIFFERENCE = \frac{2(\emptyset_1 - \emptyset_2)}{\emptyset_1 + \emptyset_2} \times 100} \quad 3\text{-}9$$

3.11 Comparative Analysis with Other Reactors and the MHTGR

The comparison with Bostelmann et al. (2016) and Flouride-Salt-Cooled (2016) was done to verify and validate the research findings by observing how they compare with established studies. This was a confirmation that the new models were being properly modelled.

Bostelmann et al. (2016) was used for comparison as well as to confirm discrepancies and the correctness of the modelling approach. It also provided insight into the behaviour of the reactors that might highlight trends, allowing for improvement and facilitating compliance with the regulations.

For the comparison with a different reactor such as Flouride-salt-cooled High-temperature Reactors, Flouride-Salt-Cooled (2016) was used to determine whether the difference between the Serpent and KENO-VI k_{eff} results will correspond to those found in Bostelmann et al. (2016).

3.12 Data Interpretation and Visualisation

- Graphics

The graphic representation is initially introduced in the verification section in Chapter 4, where the purpose is to check for any source convergence and to make sure that the KENO-VI and Serpent results are close to being equal.

This was done by using the scatter plot graph with straight lines, essentially comparing the inactive cycles using Shannon entropy results to check if they stabilise quickly with fewer or more inactive cycles. Graphs were also used in plotting the k_{eff} vs cycle. The error bars of the k_{eff} for each model should ideally overlap into each to indicate stability. Ideally, if the graph lies within the same boundaries or appears to be constant after the number of inactive cycles has passed, then stability is reached, and source convergence is obtained.

The reason for measuring the source convergence was to make sure that the neutron source was well distributed.

The use of graphics was adapted later in the study by plotting the neutron flux graphs by using information provided in the tallies. This was done using MATLAB.

- Tallies

Tallies were used to record interactions related to neutron flux, within certain regions of the reactor model, to enable an understanding of the MHTGR-350 reactor behaviour. For example, linear plots through specific directions in the core would make it easier to visualise the distribution of flux.

The purpose of tallies helps in counting specific physical events, such as:

1. Neutron flux,
2. Neutron interactions,
3. Energy deposition in fuel or moderator.

The steps taken in the tracking of neutron flux were:

1. The identification of the tally to be produced, e.g. what kind of tally would be of benefit to the work, for this work it was the flux tally.
2. Running the simulations and making sure that the tallies are set to track the relevant parameter.
3. The examination of the output by checking the neutron flux values and statistical errors.
4. The analysis of data by incorporating the plot of neutron flux across the reactor geometry where the starting point is the centre of the core and going to the outer regions. Comparison of flux in different regions helps to determine the effectiveness of neutron moderation.
5. Compare the results and the data analysed with other literature for accuracy.

- Tables

Tables were implemented to organise and interpret the data, to make it easy to compare the values and identify patterns in the results.

Additionally, the inclusion of tables was for the pre-visualisation of graphs used to check for source convergence.

3.13 Limitations of the Methodology

The limitations of the tools used are that they normally use simplifications and assumptions of models, such as ideal geometries and homogeneous material distributions, which might not represent all the distinctive features of a real reactor. Simulation codes such as Serpent and KENO-VI use statistical sampling, and thus they introduce uncertainty into the results. Due to the fact that experimental data are not available to validate calculation data, it is difficult to establish the correctness of the calculated safety parameters in line with real-life situations.

The high computational demand and time required to achieve high-accuracy results may restrict large-scale reactors. Because KENO-VI and Serpent produce results that have great variations from each other even though they are running identical models, the question regarding which one is producing accurate results if the same reactor data was used needs to be considered.

Graphs, tallies, and tables have their worth in summarising data, but the limits include their abstract nature of simulation data for complex behaviours represented by spatial flux peaking and time-dependent changes, and it requires interpretive effort beyond direct world observation. These would include rarer, safety-critical events, such as certain accident scenarios, which may not occur with sufficient frequency during simulation to be accurately represented in the tally data.

Interpreting the results require careful data analysis by experts. The nature of the data involved may be so complex that it could lead to errors in interpretation and result in incorrect conclusions on safety issues. In that respect, these tools and frameworks are ideal for reactor analysis, but they often find an optimum application when combined with experimental data, additional neutronic codes, and multidisciplinary approaches toward a comprehensive and validated safety assessment.

3.14 Summary

This chapter discussed the methodology used to achieve the aim of this dissertation. This was done by first mentioning the research approach and design, followed by the discussion of the selected reactor type. This resulted in delving deep into the set-up of the reactor and the discussion of how the safety parameters are going to be calculated, which included the method of collection of the results and the computer and software resources that will be used. The chapter concluded with the limitations of the methodology.

CHAPTER 4 RESULTS AND DISCUSSIONS

4.1 Introduction

This chapter presents the verification and validation of the Serpent and KENO-VI model. This is done using tabular and graphical representation of the results, the same representations are used to present the results from calculating the fuel and moderator temperature coefficient, along with neutron flux. In every sub-section there is a discussion of the results obtained.

4.2 Convergence

4.2.1 Source Convergence

Checking the convergence of the source before doing any calculations is important to ensure that the fission source distribution within a system has stabilised (Cheng et al., 2024). This was done by increasing the number of skipped cycles and portraying them graphically as explained in the methodology section. Note that the checking source convergence test is only applied to Serpent calculations, as the KENO-VI calculation already states in the output file whether the source has converged or not.

All the differences calculated in this section used the unit pcm, this is a reactivity unit that abbreviates to “per cent mile”. In terms of using the multiplication factor (k_{eff}) when k_{eff} is close to 1.0, the difference in k is close to that of the difference in reactivity ρ. The difference in k, when multiplied by 1×10^{-5} is then the difference (approximate but close) in pcm. In this work, the difference is calculated using k_{eff} instead of ρ to allow easier analysis, since results are listed in the output files as k_{eff} rather than ρ.

Table 4-1: Table showing the convergence of sources.

File name	skipped cycles	active cycles	Total cycles	k_{eff}		Standard deviation (σ) (pcm)
				Serpent	KENO-VI	
e020	10	400	410	1.47282	1.46141	14
e021	20	400	420	1.47288	1.46158	14
e022	50	400	450	1.47312	1.46150	14
e023	100	400	500	1.47294	1.46138	13
e024	200	400	600	1.47287	1.46143	13
e013	400	400	800	1.47280	1.46158	10
e014	800	400	1200	1.47283	1.46133	7.8
e015	1600	400	2000	1.47266	1.46153	7.7

The difference in k, when multiplied by 1×10^{-5} is then the difference (approximate but close) in pcm. In this work, the difference is calculated using $keff$ instead of ρ to allow easier analysis, since results are listed in the output files as k_{eff} rather than ρ.

Table 4-1 displays the source convergence results as an increase in the number of skipped cycles is applied. As seen in the results, the value of the standard deviation slightly decreases as the number of skipped cycles increases. The results seen in this table do not portray the progression of the results as anticipated, therefore a graphical representation of the results was introduced to illustrate the trend of the results as seen in Figure 4-1.

The tabulated graphical data are shown below:

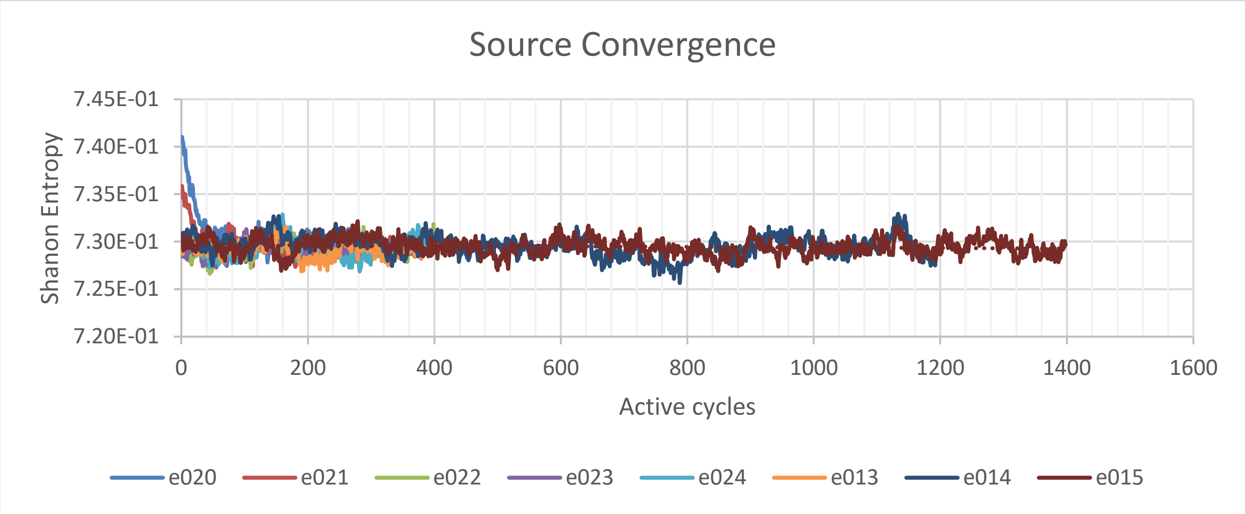

Figure 4-1: Source convergence graph using Shannon entropy.

From Figure 4-1, one can deduce that having at least 40 active cycles will result in the source to converge but it is still not quite clear. Therefore another graph is needed to clearly show how many numbers of active cycles to have in order for the source to converge and this can be seen in Figure 4-2.

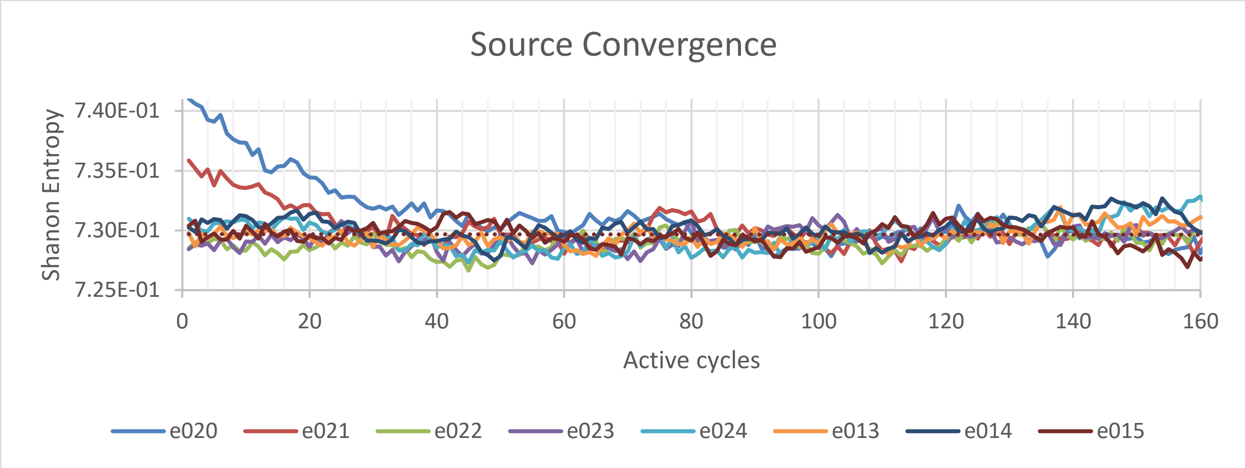

Figure 4-2: Close-up graph portraying source convergence graph using Shannon entropy.

Figures 4-1 and 4-2, display the active cycles on the x-axis and the minor grid lines are in intervals of 40. Since these are only the active cycles, for the source to be accepted to be converged, the curves must be statistically constant, i.e. straight horizontal lines with statistical fluctuations.

It is evident from the figure that tests from files e020 and e021 do not converge, and the rest can be considered to be converged. Taking into account Table 4.1, the overall number of inactive cycles for the source to converge is 50 inactive cycles, implying that for the source to converge, a minimum of 50 inactive cycles should be skipped. However, a conservative number of 300 skipped cycles are implemented to ensure accuracy and reliability.

4.2.2 Standard deviation reduction

A test was done to conclude how many active cycles should be implemented to see a noticeable difference in the standard deviation when increasing the active cycles, and the results are tabulated below.

Table 4-2: Standard deviation reduction table.

File name	skipped cycles	Active Cycles	Total cycles	k_{eff}		$\sigma\ (pcm)$
				Serpent	KENO-VI	
e045	300	100	400	1.47285	1.46173	28
e046	300	200	500	1.47358	1.46174	22
e047	300	400	700	1.47286	1.46165	15
e048	300	600	900	1.47274	1.46159	11
e051	300	800	1100	1.47276	1.46161	9.7
e049	300	2000	2300	1.47287	1.461487	6.2
e050	300	4000	4300	1.47304	Leakage	4.4

From Table 4-2, it can be deduced that increasing the number of active cycles will increase the stability and accuracy of the code and the results will be deemed more reliable due to the decrease in the standard deviation. Although the standard deviation for 2000 active cycles is higher than compared to the standard deviation of 4000 active cycles, and the difference in the multiplication factor between the Serpent results is less than 20, the KENO-VI result calculations were completed with a leakage error appearing, and therefore, it is acceptable to use the 2000 active cycles.

4.3 Comparison of the Serpent and KENO-VI Models

After selecting the inactive and active cycles for stability and accuracy, the next step was to verify the Serpent and KENO-VI input files. A set of calculations was performed to check the difference in the multiplication factor between the Serpent and KENO-VI models using model e049. It should be noted that many models were developed and numbered accordingly. The numbering does not have any acronym meaning. The number of models is given here and later for other models so that all the data can be archived and easy access to any particular model can be made.

Table 4-3: Results for the selected model after the source convergence test.

Model number	skipped cycles	Active Cycles	Total cycles	k_{eff}		σ (pcm)
				Serpent	KENO-VI	
e049	300	2000	2300	1.47287	1.461487	1138.3

The results in Table 4-3 are for the full core models. They represent a significant difference in the multiplication factor between the Serpent and KENO-VI models, and the reasons could be similar to the ones listed in Ringane (2022).

With the guidance from the literature mentioned above, an overview of the NWURCS base model was done by:

- Checking the nuclear data libraries that were used.
- Performing a detailed analysis of the geometry, and
- Verification of materials, temperatures, and densities.

4.3.1 Nuclear libraries verifications

When checking the cross-section libraries, a comparison was made between two cross-section data sets. It became evident that the Serpent calculation had made use of both the ENDF cross-section data and the JEFF cross-section data. Modifications were made to use only data from the ENDF cross-section library data and the results are recorded in Table 4-4.

Table 4-4: Results after cross-section library data modification.

File name	Temperature in K	k_{eff}		Δk_{eff} (pcm)
		Serpent	KENO-VI	
d049	300	1.47304	1.461487	1155.3

When comparing the results in Table 4-4 to those in Table 4-3, an increase of $17\,pcm$ can be seen in the multiplication factor for the Serpent code after the cross-section library data modification, while the KENO-VI results remained fixed. This increases the difference between the Serpent and the KENO-VI codes. However, this difference is less than 3 times that of the standard deviation of the calculation. Assuming a normal distribution for the standard deviation, this is acceptable. The results in Table 4-4 shows that the mixture of cross-section-library data has a small impact on k_{eff}.

Although the difference is not quite big, Bostelmann et al. (2016) highlights the importance of cross-section library data and, therefore, effort must be made to use consistent data.

4.3.2 Reducing the level schemes

Version 3 of NWURCS was significantly different from Versions 1 and 2 with the introduction of the level schemes. The verification of the level scheme for cartesian geometry was carried out by TP Ringane (2022). However, reactor designs that used hexagonal geometry for fuel blocks and unit cells (which are the hexagonal graphite matrix cells containing the compacts) were not verified previously, and the current work is the first to carry out such verification.

With the difference seen in Table 4-4, a verification needed to be performed on the input files to verify the origin of the significant difference in Serpent and KENO-VI k_{eff} results

There are numerous reasons the two input files may produce results that are far from being identical, and this section aims to find whether the geometrical assignments could have been the cause for the significant changes that were seen.

However, one should also note that two different codes can produce different results because the algorithms used in each code can be very different, together with the numerical implementation. The model was broken down systematically into homogenised levels, as explained in Section 3.7.1, to pinpoint where the large difference in the multiplication factor becomes evident. The results for the four levels were captured as follows:

Table 4-5: Results for level schemes.

File name	Level of code			σ (pcm)	Δk_{eff} between Serpent and KENO-VI (pcm)
		Serpent	KENO-VI		
q015	Level 1	1.09295	1.09188	8	107
q013	Level 2	Unable to sample fission source	1.51742	-	-
q014	Level 3	1.34202	1.34020	6.8	182
d049	Level 4	1.47304	1.46547	6.5	1174

The results seen in Table 4-5 provide an indication of the consistency of the models for the different levels of complexity. Level 1 shows the lowest difference in the multiplication factor between the Serpent and KENO-VI results. This level was the least complex and produced results with a difference of $107\ pcm$ which is $4.4 \times 3\sigma$ where σ is the standard deviation of the Monte Carlo Calculation. A difference of 3σ can be considered acceptable. The difference observed is therefore larger than what can be accepted from the statistics. Being a simple model, this difference can therefore be attributed to the use of two different codes. This means that one can expect differences of around $100\ pcm$ when using Serpent and KENO-VI because two different codes are being used.

Level 2 calculations with the utilisation of Serpent were unable to sample the fission source. A possible reason could be not being able to handle implicit fission source distributions for this particular geometry, and therefore not allowing it to run simulations in such cases. If the fission source for Serpent is not well defined, it could fail in sampling. It is shown below that level 3 homogenisation also produced small differences. Therefore, due to time constraints, the case for the level 2 comparison was not resolved. At level 3, k_{eff} diverges moderately from level 1 reaching a difference of $182\ pcm.$ This is comparable to the difference of 107 between the Serpent and KENO-VI level 1 calculations and is small compared to differences around 1100 as obtained at level 4. Therefore, it was assumed that the discrepancy (the large difference in the multiplication factor) did not arise when moving from level 2 to level 3.

When moving from level 3 to level 4 results, the results between KENO-VI and SERPENT become markedly more different.

An observation of the overall results from the table above suggests that as the homogenization decreases from levels 1 to 3 to 4, k_{eff} between KENO-VI and SERPENT increases.

When looking at the level 3 to level 4 results, there is a potential inconsistency in the results with a 715.2 increase from level 3 to level 4, indicating that the differences between the KENO-VI and SERPENT models could be in the way the model is built for the coated particles in the compact. This is the heterogeneity that is included when modelling at level 4. Level 4 is a fully heterogeneous model and is more complex than the other levels.

However, it is noted that Bostelman reports a difference of 300-450 for SERPENT versus KENO-VI calculations at this level, i.e., when the core is completely heterogeneous.

4.3.3 Comparison of Serpent and KENO results at Level 4

Having established that the modelling was correct at levels 1 and level 3, it was then concluded that the discrepancies either existed at level 4 or the transition from level 3 to level 4 (i.e. the lattice definitions). It was therefore decided to compare the Serpent and KENO-VI models, from the basic element at level 4, and to move upwards to the more complicated geometries. This meant starting with the unit cell consisting of the TRISO particle.

4.3.3.1 The single unit cell

The single unit cell is the basic building block of the HTR core. It is defined as containing the TRISO particle inside a 3D rectangular block, also called a cuboid. This is model c002 shown in the figure.

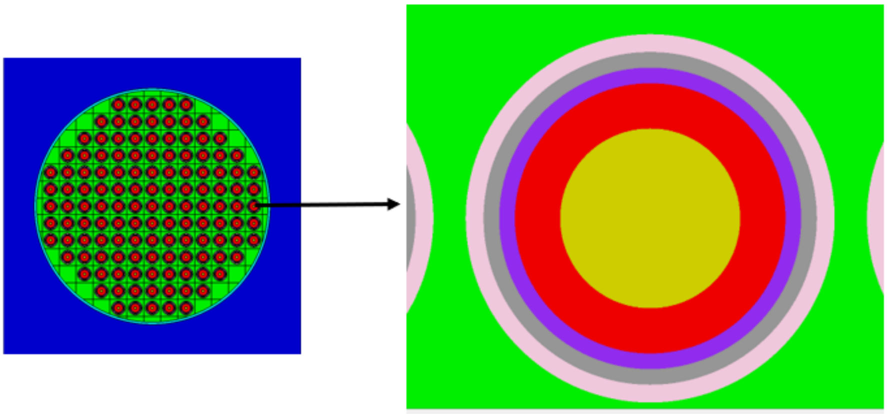

Figure 4-3: Figure showing one unit cell.

The results for the single unit cell are shown in Table 4-6.

Table 4-6: Results for 1-unit cell.

File name	Specification	k_{eff}		Δk_{eff} (pcm)
		Serpent	KEN0_VI	
c002	One unit cell	1.09218	1.09172	46

The difference in the multiplication factor seen in case c002 is slightly larger than 3σ but not greater than $50\ pcm$. This was the simplest model in terms of the TRISO particles and was easy to verify in terms of the input files. Given this, it is safe to say that the accuracy in the models for modelling one unit cell filled with fuel particles is high. This therefore places a lower limit of $50\ pcm$ on the differences that can be acceptable between the Serpent and KENO-VI results.

In general, the results seen in Table 4-6 were for one unit cell. Therefore, considering several unit cells, the difference could increase moderately.

The concern is now directed to the lattice construction. This resulted in calculations being performed, and the results of the investigation on lattices are portrayed in the next section.

4.3.3.2 Lattice construction of a compact.

The fuel compact is composed of a number of coated particles contained in a graphite matrix, as discussed in Section 4.2.3.1. One way to model these particles is to use a regular lattice. As mentioned earlier, it does not allow the randomness of the coated particles to be easily modelled, but such a construct allows for easy development of the model.

4.3.3.2.1 Axial expansion

The next step in comparing the Serpent and KENO-VI models was to check whether the construction of these lattices contributed to the differences in the multiplication factor between Serpent and KENO-VI. The modifications started with the placement of two fuel compacts in one box (lattice); note that this is an informal description, but it helps with understanding of the modifications. The modifications help to check how 2-unit cells interact with each other in one lattice. Figure 4-4 shows a graphical representation of the file f002.

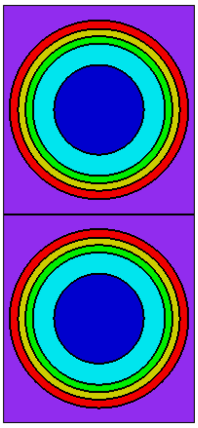

Figure 4-4: Two-unit cells in one lattice.

The results of placing two-unit cells in one lattice are tabulated below.

Table 4-7: Results for 2-unit cells in one lattice.

File name	Specification	k_{eff}		$\Delta k_{eff}\ (pcm)$
		Serpent	KENO-VI	
f002	2-unit cells in one lattice	1.09239	1.091946	44.4

The set of results in Table 4-7 portrays a difference in k_{eff} of 44.4 pcm, which is not high as it has decreased by 1.6 pcm from the results of a single unit cell. The difference in the k_{eff} further shows the alignment of the input files.

As complexity increases, an addition of 48 more unit cells in a single lattice to check how 50 fuel elements that are vertically placed in one lattice interact with each other. Figure 4-5 below shows the modification for clarity.

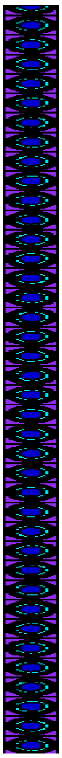

Figure 4-5: Side view of fuel cells stacked on top of each other in one lattice.

The results of axially placing 50-unit cells in one lattice are presented in Table 4-8.

Table 4-8: Results for 50-unit cells in one lattice.

File name	Specification	k_{eff}		$\Delta k_{eff}\ (pcm)$
		Serpent	KENO-VI	
f020	50-unit cells in one lattice	1.09206	1.09195	11

Table 4-8 shows the multiplication factor difference being $11\ pcm$. This implies that the results are more or less close to being equal and there is not much difference in the Serpent and KENO-VI input files when it comes to axially modelling 50-unit cells in one lattice.

Having established that the axial stacking of the 50-unit cells did not show significant changes between the Serpent and KENO-VI models, the radial expansion of the model was considered.

4.3.3.2.2 Radial expansion

The previous modification was a $1 \times 1 \times 50$ lattice, radial expansion focusses on a $15 \times 15 \times 50$ lattice, meaning that an addition of 15 unit cells is added in the x and y-direction and 50 unit cells in the z-direction, so in total there are 225 lattice cells in the x-y plane and 129 of those cells each have a fuel TRISO particle with 50 fuel cells stacked axially as seen in Figure 4-6.

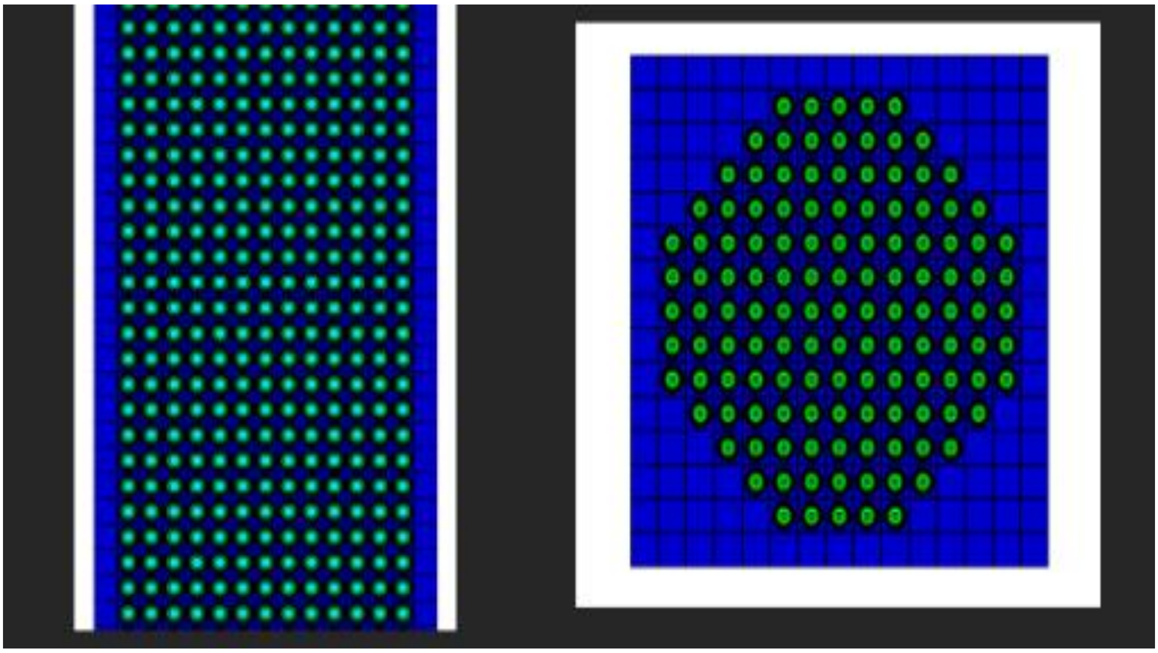

Figure 4-6: Front and top view of the rectangular fuel compact.

The k_{eff} results for the $15 \times 15 \times 50$ lattice are displayed below.

Table 4-9: Results for $15 \times 15 \times 50$ rectangular compact.

File name	Specification	k_{eff}		$\Delta k_{eff}\ (pcm)$
		Serpent	KENO-VI	
f042	A rectangular compact of dimensions 15x15x50	1.21317	1.21248	69

Although the results in Table 4-9 display a relatively larger increase than the single line axial placement of 50-unit cells, Δk_{eff} is relatively low. In terms of statistical error, the difference was about 9σ.

Before examining the lattice structure of a fuel compact, calculations were done to see the effect of a cylindrical gap filled with helium on k_{eff}, given that the compact placed in the fuel block requires an addition of this gap. Figure 4-7 displays this addition; the gap is represented by a dark blue circle surrounding the $15 \times 15 \times 50$ lattice structure.

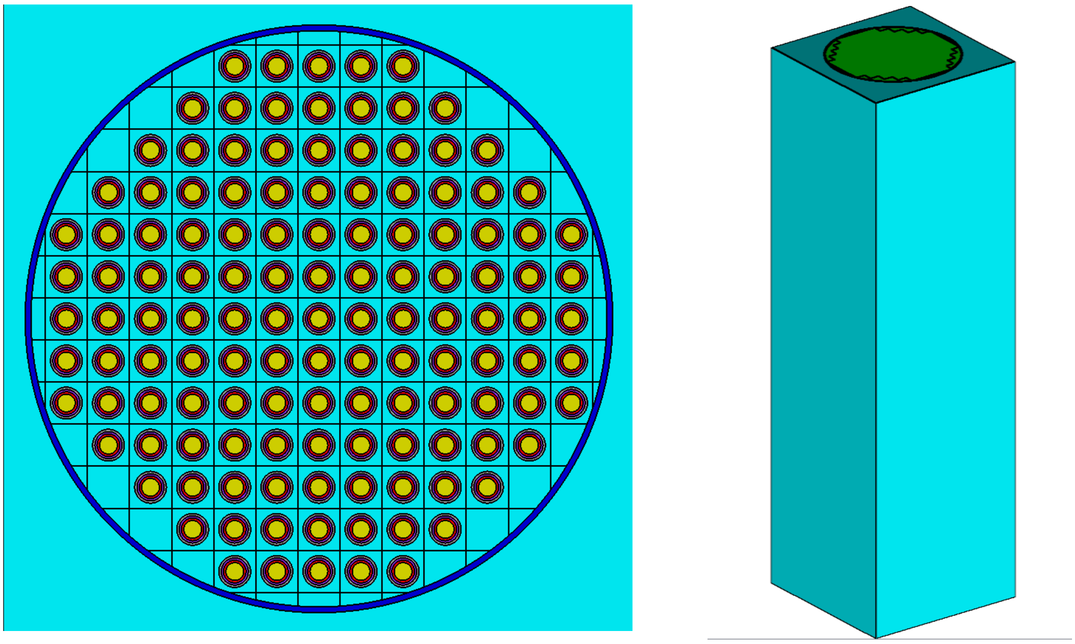

Figure 4-7: Top and 3D view of the fuel compact surrounded by a helium-filled gap.

The results for the addition of the helium gap are tabulated below.

Table 4-10: Results of inserting a cylindrical helium-filled gap.

File name	Specification	k_{eff}		$\Delta k_{eff}\ (pcm)$
		Serpent	KENO-VI	
g020	• Put f042 inside a cylinder • Insert gap between material 53 and cylinder	1.20553	1.20471	82

The difference in the results is not big, therefore, the large difference seen in b002 is not caused by the inclusion of a helium gap.

The results seen from the construction of a unit cell to the addition of a helium gap surrounding the fifteen 50-unit cells have been increasing moderately. This shows that there is no problem with the unit cells and the construction of the fuel compacts. Therefore, the next step taken was to reconstruct a ‘fuel rod’.

4.3.3.3 Reconstructing and analysing a single ‘fuel rod’

The fuel compacts in Section 4.2.3.2.2, are stacked one on top of each other in a fuel channel of the hexagonal graphite block, shown in Figure 4-7. Note that in this model, the entire graphite block is not yet modelled, only that part that constains the fuel channel. This compact stack can be compared to a PWR fuel rod and can be labelled as a ‘fuel rod’. Next, the effect of this stacking on the differences between the Serpent and KENO-VI calculations was considered.

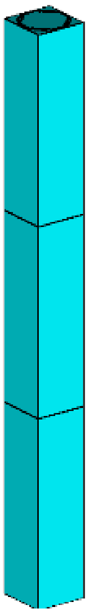

Figure 4-8: Three fuel compacts stacked on top of each other.

The addition of two more fuel compacts to a single fuel compact has given the following results:

Table 4-11: Results for three fuel compacts.

File name	Specification	k_{eff}		Δk_{eff} (pcm)
		Serpent	KENO-VI	
h002	Three fuel compacts stacked on top of each other.	1.20555	1.20499	56

A 56 pcm difference is recorded, this is a small difference between Serpent and KENO-VI results, and it is acceptable. It is not much of a difference in the k_{eff} such that it could raise concerns.

More fuel compacts were added; this time an addition that resulted in six fuel compacts. Figure 4-9 shows the image of the six fuel compacts.

Figure 4-9: Six fuel compacts stacked on top of each other.

The results for the stacking of six fuel compacts are shown below:

Table 4-12: Results for axially stacking six fuel compacts.

File name	Specification	k_{eff}		Δk_{eff} (pcm)
		Serpent	KENO-VI	
h004	Six fuel blocks stacked each other.	1.20561	1.20499	97

The six fuel compacts result in a 97 pcm difference in the multiplication factor between Serpent and KENO-VI and this compared to results in Table 4-12 has increased by 41 pcm. From the construction of one fuel compact, these results have been moderately increasing. Therefore this difference does not raise any suspicion regarding the lattice structure of six axially stacked fuel compacts.

More fuel compacts were added as seen in the Figure 4-10 below.

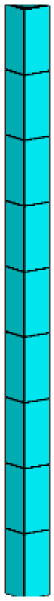

Figure 4-10: Nine fuel blocks axially stacked.

The results are shown in Table 4-13.

Table 4-13: Results for axially stacking nine fuel compacts.

File name	Specification	k_{eff}		$\Delta k_{eff}\ (pcm)$
		Serpent	KENO-VI	
h006	Nine fuel compacts blocks are axially stacked.	1.20545	1.20463	53

The k_{eff} difference between Serpent and KENO-VI is 53 pcm, this result as seen with other differences is minimal therefore it is appropriate.

Finally, the full fuel rod is implemented next, which contains 15 fuel compacts with the addition of bottom and top caps.

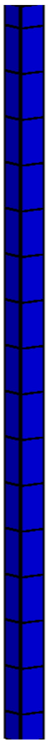

Figure 4-11: Fifteen fuel blocks axially stacked with bottom and top caps.

The results for the "fuel rod" with bottom and top caps are tabulated below.

Table 4-14: Results for a 'fuel rod' that consists of fifteen fuel compacts with bottom and top caps.

File name	Specification	k_{eff}		Δk_{eff} (pcm)
		Serpent	KENO-VI	
g022	15 block stacks axially stacked with the inclusion of bottom and top caps	1.23861	1.23778	106

Table 4-6 to Table 4-14 show the difference of moving from a unit cell (TRISO particle in cuboid cell) to a fuel compact and finally to a 'fuel rod'. The results from the single fuel compact to a 'fuel rod' show a trend in the difference of Δk_{eff} where smaller geometries improve consistently in the two models. Although that is not the case for file h006 with fewer fuel compacts, the trend remains valid because of what a lot of results have portrayed. Given that the geometry of the stacked blocks was rectangular, it was also easy to compare the Serpent and KENO-VI input files, and no errors were found. Both models used a lattice scheme to define the 15 blocks. The difference could therefore be due to the statistical process when characterising neutron transport through a lattice (most probably through lattice walls). Therefore, it can be concluded that there is no fault in the lattices and units.

4.3.3.4 Analysis of a hexagonal 'fuel rod' and neutron leaks

The next step in the analysis at level 4 was to change from the cuboid fuel rod to the hexagonal fuel rod, since hexagonal cells are used in the lattice for the fuel graphite block. In this model, the compact and gap remained cylindrical, whilst the outer surface needed to be changed from rectangular to hexagonal.

However, it needs to be pointed out at this stage, that an error in the output was observed for the heterogenous full core model at cycle 255, 653 and other cycles, as shown in Figure 4-12 and Figure 4-13.

Experience of the NWURCS code developer with MCNP modelling (which is another Monte Carlo code used for neutron transport similar to KENO-VI and Serpent) indicates that this could be due to the phenomenon of numerical truncation. In MCNP, if two bodies are positioned next to each other, with a common surface (a plane for example), then both these bodies must be defined using a common surface. If two surfaces were used, then 'lost particles' could arise. For example, assume that the surface is a plane at position 18.0100. Then if two planes are used, both defined at 18.0100, then the left plane might be defined computationally as 18.0100010 and the right plane might be defined as 18.0100020. There then exists a region of 0.0000010 between these two planes that are not defined, and when a neutron lands in this region, it is considered as a "lost particle" in MCNP and an error is given.

It is possible a similar problem as arisen in KENO-VI, where in the current model a composite body is used to define the hexagon. The test would be to define the hexagon by six planes; these common planes then become shared between neighbouring hexagons, and to check if the error still persists. However, such work was considered beyond the scope of the present project by the NWURCS code developer and has been reserved for resolution in a future project.

The high difference between the Serpent and KENO-VI models of around 1100 pcm could therefore not be resolved if it is due to geometry. However, the analysis in the previous sections confirms that much of the model between the two inputs are consistent.

```
     254       1.45984E+00      1.46126E+00      1.99965E-04      5.
     255       1.46009E+00      1.46126E+00      1.99574E-04      5.

****** error *****keno message number k6-242 follows:
neutron 56577 in generation 256 has leaked from unit 374
at x =    -6.72963E-01 y =     9.09218E-01 z =     1.28600E+01
but is still within the volume defined by the unit boundary record.
     256       1.46264E+00      1.46126E+00      1.98018E-04      5.
     257       1.46099E+00      1.46126E+00      1.96525E-04      5.
```

Figure 4-12: Error message for the heterogenous full core KENO-VI model in generation 255.

```
       653        1.46131E+00       1.46120E+00       9.57222E-05       5.

 ****** error *****keno message number k6-242 follows:
 neutron 35953 in generation 654 has leaked from unit 304
 at x =    -9.56728E-01 y =     3.85871E-01 z =     2.76500E+01
 but is still within the volume defined by the unit boundary record.
       654        1.45566E+00       1.46119E+00       9.60714E-05       5.
       655        1.45813E+00       1.46118E+00       9.60560E-05       5.
```

Figure 4-13: Error message for the heterogenous full core KENO-VI model in generation 653.

4.4 The impact of thermal scattering

According to Atkinson et al. (2021) and Zu et al. (2021) , thermal scattering that is linked to coolant materials increases the accuracy when bound atoms are used; this shows the importance of thermal scattering in water reactors. Although thermal scattering in water reactors is with water and for gas-cooled reactors, graphite is the scatterer, the findings from Atkinson *et al.* (2021), prompted a re-examination of the input data to see the impact of thermal scattering in the MHTGR-350 model. During this re-examination, it was discovered that the inclusion of thermal scattering in the Serpent input file was omitted. On the other hand, Bostelmann et al. (2016) states that in SCALE 6.2 the beta version includes a new 252-group library that provides, amongst others, an increase in the thermal scattering cut-off, implying that the inclusion of thermal scattering had already been implemented in previous versions and now has been improved to treat low-energy neutrons accurately. Another test was also carried out to check whether thermal scattering was included in the cross-section library when running KENO-VI. SCALE is distributed with a set of input decks that the user can use when building his/her own models. Some of these are input for HTR reactors with one example being “csas6_randomgeom.inp.DISABLED”. Examination of this file did not show any explicit modelling of thermal scattering. However, it was noted that the syntax “c-graphite” instead of “c” must be used in the “composition” block. This was already implemented in the NWURCS generated input.

Therefore, since SCALE-6.2 had already implemented thermal scattering, calculations were only employed for the Serpent input, and the results are tabulated below.

The ticks in the boxes represent what has been included in the Serpent input code.

Table 4-15: Table showing the results for Serpent to see the effect of thermal scattering.

File name	o-uo-10t	o-uo-11t	u-uo-10t	u-uo-11t	grph gre7.00t	Multiplication factor results
d049					✓	1.47304
x005	✓	✓	✓	✓	✓	error
x106	✓	✓		✓	✓	1.47267
x107	✓	✓	✓		✓	1.47297
x108	✓			✓	✓	1.47287
x109		✓		✓	✓	1.47294
x111	✓		✓		✓	1.47276
x112		✓	✓	✓	✓	error
x113	✓		✓	✓	✓	error
x114		✓	✓		✓	1.47278
x116						1.47701

In the table above, the thermal data sets of o-uo-10t and u-uo-10t are at $294\ K$ and o-uo-11t and u-uo-11t are at $400\ K$. The temperature for the models used in this work was the cold case, at $300\ K$. When specifying both data sets, Serpent uses an intermediate value for the thermal scattering data, suitable to the temperature required.

The table above concludes that U-Uo-10t and U-uo-11t do not work together due to the errors they produce, but they work on their own. This could be a result of the inability for Serpent to process both entries simultaneously. However, O-Uo-10t and O-uo-11t work even by including both entries simultaneously. Since the input file syntax for both the oxygen isotopes and the uranium isotopes are the same, it is possible that the error lies in the processing of the uranium isotopes by Serpent.

The following table show the differences in the outputs for every file in Table 4-16.

Table 4-16: Table showing the Serpent results after the inclusion of thermal scattering.

File name	Serpent multiplication factor results	The difference in the multiplication factor from b002 Δk_{eff} (pcm)
d045	1.47304	Reference
x005	Error	N/A
x106	1.47267	37
x107	1.47271	33
x108	1.47287	17
x109	1.47294	1
x111	1.47276	28
x012	error	N/A
x013	error	N/A
x114	1.47278	26
x116	1.47701	397

Table 4-16 shows a very minimal multiplication factor (k_{eff}) difference in the models compared to the base model for the oxygen and uranium scatterers, indicating that the inclusion of these thermal scatterings in the Serpent input file does not affect the multiplication factor (k_{eff}) . They should, however, be included for a technically correct input deck. It is also seen that there is a difference of $30\,pcm$ when using u-uo-10t or u-uo-11t cross-section data sets, which are calculations x106 and x107. Since this is equal to 3σ, it is accepted that either cross-section data set can be used. However, x106 would be more appropriate since $300\ K$ is closer to $294\ K$ than $400\ K$.

There is a $397\ pcm$ decrease in the results with the exclusion of graphite thermal scattering. From this kind of difference, what can be said about the inclusion of the graphite thermal scattering is that:

- It changes the accuracy of the model,
- It shows the dependence of neutron moderation on the contribution of graphite thermal scattering.

This suggests that the thermal scattering of graphite should not be neglected.

The modifications that have been done thus far are those that include the ENDF nuclear library cross-section data and the necessity of including graphite thermal scattering, therefore the results are still those of case d049. These are presented again in Table 4-17

Table 4-17: Difference in multiplication factor after comparisons of Serpent and KENO-VI.

File name	Temperature	k_{eff}		$\Delta k_{eff}\ (pcm)$
		Serpent	KENO-VI	
d049	300	1.47304	1.461487	1138.3

4.5 Verification of other data required by NWURCS

The analysis of the given Serpent model is done by comparing each characteristic and parameter (Ortensi *et al.*, 2015). The reason for doing these comparisons is that the model in Ortensi's work was used to construct the model in this dissertation.

This section will help in providing what aspects of the model that is used in this dissertation need to be adjusted to ensure greater accuracy within the results. However, there are parameters that are required in NWURCS that are not required for neutronic analysis but are required for other analyses such as thermal fluid analysis (often referred to as by the misnomer thermal hydraulics analysis). These parameters are also discussed.

It is important to note that during the verification process, the input file named d049 is referred to as the base model that was given, unless stated otherwise.

The comparison revealed a few discrepancies in Table 2-4 which are listed in the table below.

Table 4-18: Table showing the Parameters and Characteristics that deviate from Ortensi *et al.* (2015)

MHTGR-350 Characteristics	**Value in base case d049**	**Value from** Ortensi et al. (2015)
Reactor Power	$300\ MW(t)$	$350\ MW(t)$
Installed electric capacity	$141.428\ MW(e)$	$165\ MW(e)$
Primary coolant pressure	$2.400E+05\ Pa$	$6.39E+06\ Pa$
Core outlet temperature	$650\ K$	$960\ K$
Core inlet temperature	$300\ K$	$532\ K$
Mass Flow Rate	$171.00\ kg/s$	$157.1\ kg/s$
Reactor Vessel Height	$9.9126\ m$	$22\ m$
Reflector Diameter	$6.346\ m$	$6.8\ m$

According to the theory in Lamarsh & Baratta (2014), thermal power is the rate at which heat is produced in the reactor core due to reactions such as the fission reaction in the fuel; these fission reactions are known to be characterised by neutronic calculations. However, in the Serpent calculation, the number of neutrons per generation is input by the user using suitable insight to give a well-converged fission source as monitored by the Shannon entropy. The thermal power is used to quantify the flux that is tallied. It does not affect the Monte Carlo process directly. Therefore, in this study, the exact specification of the thermal power is not required, and the difference can be ignored. However, for studies that focus on thermal calculations, this difference needs to be adjusted so that the flux and power output from the Serpent calculations are of the correct magnitude.

Another discrepancy is seen in the second characteristic listed in the table above 'installation of electric capacity'. The characteristic describes the electric capacity at which the reactor is installed and, logically, the two characteristics are interconnected in the sense that the electrical power depends on thermal capacity and efficiency. Therefore, it will also not have an impact on neutronic calculations for this study.

Another difference includes the primary coolant pressure between the two models. The coolant pressure in the original model is given as $2.400E + 05\ Pa$, whereas the one given by Ortensi et al. (2015) is $6.39E + 06\ Pa$. The coolant pressure influences both the coolant density and temperature.

The core inlet and outlet temperatures were also different. However, the reactor models used in this study were isothermal models, with temperatures set at $300\ K$. This state would represent the reactor with fresh fuel just before start-up.

Given that the pressure in a system will affect the density of the fluid of the system, calculations were done using the pressure given by Ortensi et al. (2015) to investigate how the coolant density influences the neutron behaviour.

To calculate the coolant density for Ortensi et al. (2015), the use of the ideal Gas Law was implemented where,

P = Pressure in pascals,

V = Volume in cubic meters which is assumed to be 1,

n = Number of moles per unit volume,

R = Ideal gas constant (8.314 J/mol· K),

T=Temperature in Kelvin.

Verification was needed using the pressure value found in Ortensi et al. (2015) to ensure that the correct density was used in the original model. Upon calculating the density, a mismatch that could have been caused by human error was found revealing the density in the original model being, $0.00038488\ g/cm^3$ instead of $0.00151981\ g/cm^3$. To check the impact that this discrepancy had on the neutronics by evaluating the k_{eff} of both densities using the same pressure, another model (file y101) was created. The results are tabulated below.

Table 4-19: Table showing the Serpent results with the same pressure and density as Ortensi et al. (2015) model.

File name	Description	$\Delta k_{eff}\ (pcm)$	$\Delta k_{eff}\ (pcm)$
d049	Pressure is 2.400E+05Pa and density is $0.00151981\ g/cm^3$	1.47304	reference
y101	Pressure is 2.400E+05Pa and density is $0.00038488\ g/cm^3$	1.47281	3
y102	Pressure is 6.390E+06Pa and density is $0.01025444\ g/cm^3$	1.47282	4

From the above, the deduction that the density of helium gas coolant does not have any significance in k_{eff} can be made. Although coolant density can be an important aspect in thermal-fluids analysis, its role in neutronics and its influence on k_{eff} can be neglected in these cases.

Another characteristic that is different from the one in Ortensi et al. (2015), is the core inlet and outlet temperatures. This characteristic is explained using the isothermal cold case start-up. An isothermal cold case as mentioned earlier is a start-up plant state that assumes a uniform temperature. Generally, all components of the reactor are assumed to be at the same uniform initial temperature. In this case, “cold”, is interpreted as an ambient (low temperature) condition relative to a normal operation state for a reactor, making it appropriate for baseline analysis. This means that during this period, fission reactions do not produce heat, and the reactor is under fully controlled conditions. This condition serves as the start-up sequence that will evolve to increasing temperatures. This explains the reduced inlet and outlet temperatures compared to those found in Ortensi et al. (2015).

Similarly to the thermal power and primary coolant pressure, mass flow rate primarily affects thermal-fluids aspects, because since neutronic calculations depend primarily on material properties, geometry, and nuclear cross-sections, the mass flow rate holds no significance in neutronic behaviour for steady-state conditions. However, as mentioned previously, many characteristics need to be adjusted and set to ensure that a consistent model is ready for any kind of study.

Finally, the two last characteristics from Table 4-19 are the reactor vessel height and diameter. The difference shown is due to neutronic models needing to be bounded because the larger the model, the more expensive it gets computationally to get results for k_{eff}.

In the context of neutronic modelling, bounding is defined in this sense as the process of reducing the physical geometries to avoid higher computational costs. This is appropriate since larger models are more expensive in computation. The process of bounding is to make sure that the modelled system captures all significant neutron interactions and avoids geometric extensions that are not necessary and have little to no importance on the neutronics. This explains the reason for the original model having a smaller boundary both in height and circumference.

Calculations were done to check if the bounding to achieve the model for this dissertation was done correctly by comparing the k_{eff} Serpent results of the two models with their respective heights and diameters of their reactor vessels. The results are presented in the table below.

Table 4-20: Table showing the K_{eff} Serpent results with the same reactor vessel height and reflector diameter as Ortensi et al. (2015) model.

File name	Description	k_{eff}	Δk_{eff} (pcm)
d049	Reactor vessel height is 9.9126m and reflector diameter is 6.346m	1.47304	Reference
y203	Reactor vessel height is 22m and reflector diameter is 6.346m	1.47300	4
y204	Reactor vessel Height is 9.9126m and reflector diameter is 6.8m	1.47372	68

The results displayed in Table 4-20 show that the size of the reactor vessel has an effect on k_{eff}, given that the statistical uncertainty of the problem is less than 10 pcm. It is worth noticing that an increase in the height and diameter of the reactor vessel relative to the base model d049, yields a multiplication factor (k_{eff}) difference of 4 and 68 pcm, respectively. Although the k_{eff} difference between the increase in reactor vessel diameter, compared to the increase in reactor vessel height is larger, the relative change in the dimension was smaller (122% for the height and 7% for the diameter).

Since the reactor vessel diameter defines the diameter of the core barrel, it is therefore recommended that more attention be given to the base model in terms of accurately defining the core barrel and the region up to the core barrel. (In this model, the core barrel was not included). Further work was not carried out since the model also needs the definition of the core barrel, the down comer, and the RPV, and this was left as future work. In terms of the height of the model, 22.0 m as given by Ortensi can be taken as the upper limit. A few more calculations were conducted with values between 9.9126 m and 22.0 m as shown in Table 4-21.

Table 4-21: Results for checking the significance of reactor vessel height.

File name	Core height (m)	k_{eff}	Standard deviation (σ) (pcm)
d049	9.9126	1.47304	6.5
y207	10.0	1.47316	6.2
y208	12.0	1.47319	6.1
y209	15.0	1.47319	6.3
y203	22.0	1.47300	6.2

From Table 4-22, it can be seen that between the height of 9.9126 to 22.0 m, there is no significant change in the mulitiplication factor. Therefore, the height of 9.9126 m can be used for neutronic analysis.

In Table 2-3**,** there is only one parameter that is different from the one in Ortensi et al. (2015); it is tabulated below.

Table 4-22: Table showing the characteristics that deviate from Ortensi et al. (2015) model.

Core Parameter	**Number of fuel compacts in base case d049**	**Number of fuel compacts** (Ortensi *et al.*, 2015)
Compacts per core	2035800	2025000

In Table 4-22, it is evident that the number of compacts per core in the model used in this dissertation is higher than that found in Ortensi et al. (2015). This amounted to six additional compacts per fuel block, which can be considered significant. However, these compacts were placed within the fuel channels in the fuel block, and by using the symmetry of the geometry, they could not be changed. A more detailed analysis was required, taking into account the asymmetry that would be used. Given the time limit in terms of the scope of this project, this effect was left for further study.

Table 4-23: Table showing more characteristics that deviate from Ortensi's model.

Fuel Element Geometry	**Value**	**Value from** Ortensi et al. (2015)
Block graphite density	1.74 g/cm^3	1.85 g/cm^3

It was also found that the density of the block graphite used was different from that given by Ortensi et al. (2015). Adjustments were made to correlate the value of graphite density value with the one in Ortensi et al. (2015). This was done to assess the impact of this characteristic on neutronics by recording the k_{eff}. The Serpent results are as shown in the following table:

Table 4-24: Table showing the k_{eff} Serpent results with the same block graphite density as Ortensi's model.

File name	**Description**	**k_{eff} Serpent results**	**Difference from base case d049 (pcm)**
d049	Original model with block graphite density as *1.74*g/cm^3	1.47304	
y206	Original model with block graphite density as *1.85*g/cm^3	1.47292	12

From the results an observation of a difference of 12 pcm was recorded. The difference is insignificant; without changing the density the model will still yield adequate results.

4.6 Safety parameter calculations

The purpose of this dissertation is to generate a neutronic model for the MHTGR-350 SMR for regulatory research. As a start for regulatory research, the identification of parameters that could be studied within the framework of this study and that had an effect on neutronics was carried out, and calculations were performed. The results of these calculations can be seen in the tables below.

4.6.1 Temperature coefficient

The first calculations done after the verification process was calculating the temperature coefficients where constant temperature throughout all the included materials was used to signify the start of the reactor as seen in Figure 4-14.

```
% ----------------------------------------------------------------------
mat  m_00001  0.08725570  tmp= 301.00  moder  grph  6000  % inputmat id  51
   6000.03c  1.0000E+00
mat  m_00002  0.08725570  tmp= 301.00  moder  grph  6000  % inputmat id  52
   6000.03c  1.0000E+00
mat  m_00003  0.00001791  tmp= 301.00                     % inputmat id   2
   2003.03c  1.0100E-06
   2004.03c  1.0000E+00
mat  m_00004  0.00024050  tmp= 301.00                     % inputmat id  12
   2003.03c  1.0100E-06
   2004.03c  1.0000E+00
mat  m_00005  0.08725570  tmp= 301.00  moder  grph  6000  % inputmat id  53
   6000.03c  1.0000E+00
mat  m_00006  0.07090440  tmp= 301.00  moder uabc 92238 moder oabc 8016 % inputmat id  21
   6000.03c  1.6667E-01
   8016.03c  4.9981E-01
   8017.03c  1.9000E-04
  92235.03c  5.2224E-02
  92238.03c  2.8111E-01
mat  m_00007  0.05014700  tmp= 301.00  moder  grph  6000  % inputmat id   7
   6000.03c  1.0000E+00
mat  m_00008  0.09527920  tmp= 301.00  moder  grph  6000  % inputmat id   8
   6000.03c  1.0000E+00
mat  m_00009  0.09613680  tmp= 301.00                     % inputmat id   9
   6000.03c  5.0000E-01
  14028.03c  4.6111E-01
  14029.03c  2.3425E-02
  14030.03c  1.5460E-02
mat  m_00010  0.09527920  tmp= 301.00  moder  grph  6000  % inputmat id  10
   6000.03c  1.0000E+00
therm grph 301.0 gre7.00t gre7.04t
therm uabc u-o2.11t
therm oabc 301 o2-u.10t o2-u.11t
% ----------------------------------------------------------------------
```

Figure 4-14: Input file with isothermal temperatures for temperature $301\ K$.

In calculating the reactor coefficient, two temperature points close to each other must be chosen, and Equation **2-1** is restructured such that:

$$\propto_{\mathrm{T}} = \frac{k_2 - k_1}{T_2 - T_1}\,.$$

For linear behaviour, the above equation will be exact; however, for non-linear systems, the above equation should approximate the tangent to the curve at the point in question.

One notes however, that k_{eff} is calculated using the Monte Carlo method, and the statistical variation is also required to be considered. Therefore, if the system is non-linear, obtaining the tangent will be difficult.

As discussed in Section 3.8, therefore, five additional temperatures were used, which were considered to be close to the point in question $(300\ K)$.

Table 4-25: Results for isothermal temperature changes.

File name	Temperature in K	k_{eff} Serpent	Standard deviation (σ)	Δk_{eff} in Serpent results
a010	300	1.48411	0.000063	reference
a011	301	1.48384	0.000061	-27
a012	302	1.48358	0.000063	-53
a013	303	1.48370	0.000064	-41
a014	304	1.48361	0.000063	-50
a015	305	1.48334	0.000064	-77

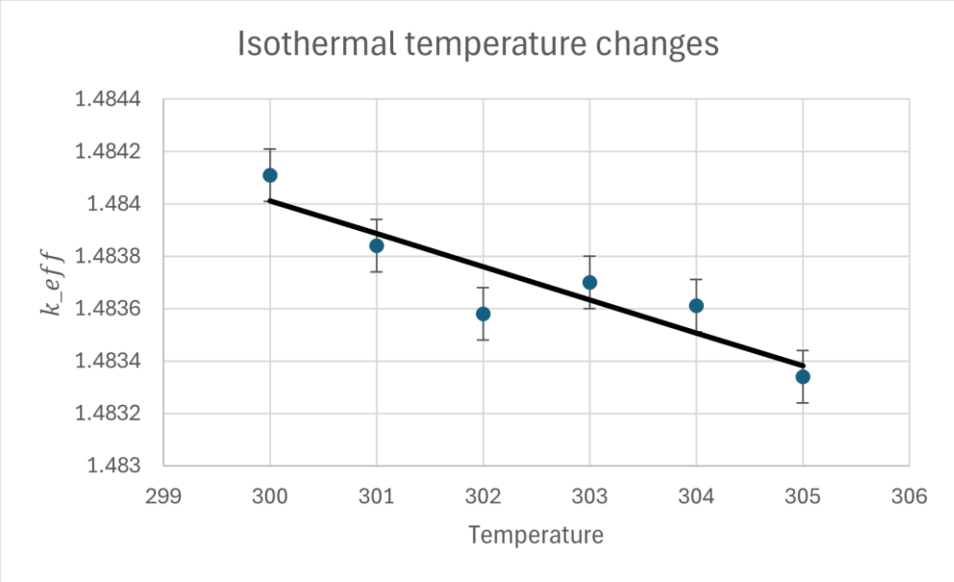

Figure 4-15: k_{eff} of isothermal temperature changes.

The results of the isothermal temperature changes are shown in Table 4.28 and in Figure 4-15. The error shown in the figure is the standard deviation as calculated by the Monte Carlo code Serpent. It can be seen that the data shows significant changes as a function of temperatures.

A linear fit was carried out on the data as discussed in section 3.8. The fit through the six data points are shown in Figure 4-15 with the equation $y = -0.00013x + 1.52189$ and the residual is calculated as 0.000246.

The line passes through all the points excluding when $T = 302\ K$, when one considers the error bars as well.

The slope of the line is -0.00013, which is the reactivity coefficient.

To calculate the error for the slope Equation **3-7** and **3-8**, were used.

From the results, the regression line for isothermal temperature increase is given by:

$$y = -0.00013x + 1.52189$$

The error of regression line is calculated using Equation 2-1 and given as:

$$\boldsymbol{\sigma_y} = 0.000123$$

Here, the errors for the coefficients **A** and **B** are calculated using Equation **3-7** and **3-8** and they are calculated as:

$$\boldsymbol{\sigma_A} = 0.00890$$

And

$$\boldsymbol{\sigma_B} = 0.0000294$$

It is noted that the error calculated for **B** is 0.00003. Then the value for reactivity is

$$\alpha_{ISO} = -0.00013 \pm 0.00003$$

Where α_{ISO} is the isothermal reactivty coefficient

If one considers only the first two data points, then the value is -0.00027 which is nine times that of the error of $\boldsymbol{B}$, and if one considers the first and sixth points, the value is -0.00077 which is 26 times that of the error in b. Given these large factors in terms of the error in $\boldsymbol{B}$, it might be best to use B with its error as determined by the linear least squares fit for the value.

It is also noted that if one uses three times the error of k_{eff} as a guide, the point at $305\ K$ could be considered to be statistically equal to the value at $300\ K$.

The interpretation is then that given the statistical uncertainty of the Monte Carlo calculation, which then appears as 0.00003 in the uncertainty of **B**, the reactivity can be negative or positive, within the bounds of $(-0.00003, 0.00003)$.

4.6.2 Fuel Temperature Coefficient

The second set of calculations done was to calculate the fuel temperature coefficient, where all materials excluding the material that included the fuel had a constant temperature of $300\ K$ displaying the beginning of the fission process, the input can be seen in Figure 4-16.

```
% ----------------------------------------------------------------------
mat  m_00001  0.08725570  tmp= 300.00  moder  grph  6000  % inputmat id  51
   6000.03c  1.0000E+00
mat  m_00002  0.08725570  tmp= 300.00  moder  grph  6000  % inputmat id  52
   6000.03c  1.0000E+00
mat  m_00003  0.00001791  tmp= 300.00                     % inputmat id   2
   2003.03c  1.0100E-06
   2004.03c  1.0000E+00
mat  m_00004  0.00024050  tmp= 300.00                     % inputmat id  12
   2003.03c  1.0100E-06
   2004.03c  1.0000E+00
mat  m_00005  0.08725570  tmp= 300.00  moder  grph  6000  % inputmat id  53
   6000.03c  1.0000E+00
mat  m_00006  0.07090440  tmp= 301.00  moder uabc 92238 moder oabc 8016 % inputmat id  21
   6000.03c  1.6667E-01
   8016.03c  4.9981E-01
   8017.03c  1.9000E-04
  92235.03c  5.2224E-02
  92238.03c  2.8111E-01
mat  m_00007  0.05014700  tmp= 300.00  moder  grph  6000  % inputmat id   7
   6000.03c  1.0000E+00
mat  m_00008  0.09527920  tmp= 300.00  moder  grph  6000  % inputmat id   8
   6000.03c  1.0000E+00
mat  m_00009  0.09613680  tmp= 300.00                     % inputmat id   9
   6000.03c  5.0000E-01
  14028.03c  4.6111E-01
  14029.03c  2.3425E-02
  14030.03c  1.5460E-02
mat  m_00010  0.09527920  tmp= 300.00  moder  grph  6000  % inputmat id  10
   6000.03c  1.0000E+00
therm grph 300.0 gre7.00t gre7.04t
therm uabc u-o2.11t
therm oabc 301 o2-u.10t o2-u.11t
% ----------------------------------------------------------------------
```

Figure 4-16: Input file with an increase in fuel temperature for temperature 301K.

Similarly to the calculations on the isothermal temperature coefficients, an observation on the effect of temperature was done using five different temperatures. As seen in the calculations of the temperature coefficient, these temperatures are also used to better understand the variation of temperature on reactivity. The results are shown in Table 4-26, with the Figure 4-17.

Table 4-26: Results for changes in fuel temperature.

File name	Temperature in K	k_{eff} Serpent	Standard deviation (σ)	Δk_{eff} in Serpent results
a010	300	1.48411	0.000063	reference
a016	301	1.48397	0.000062	-14
a017	302	1.48377	0.000063	-34
a018	303	1.48362	0.000062	-49
a019	304	1.48361	0.000063	-50
a020	305	1.48330	0.000064	-81

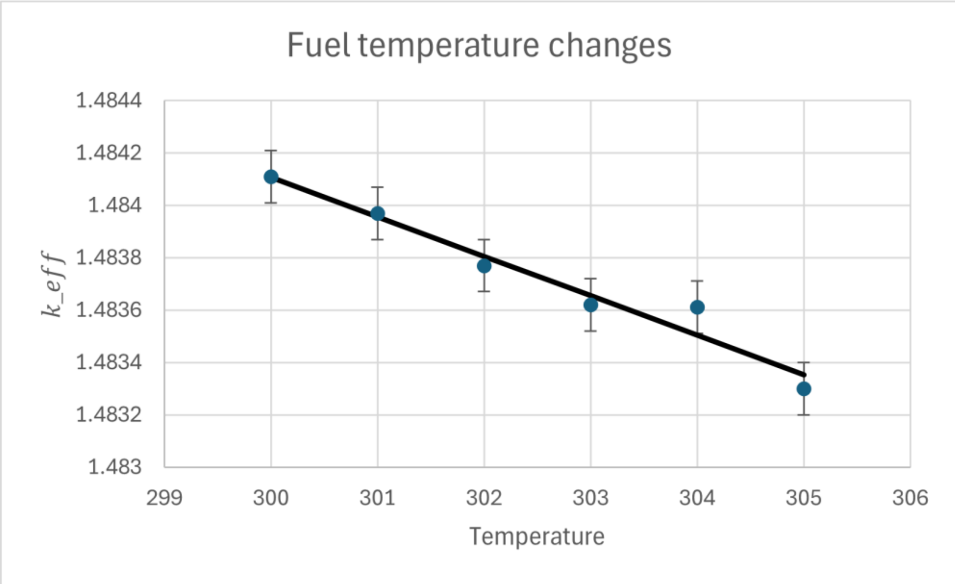

Figure 4-17: Figure displaying results for fuel temperature changes.

A linear fit with equation $y = -0.00015x + 1.529364$ that passes through the six data points is shown with a residual of 0.000129. The line passes through all the points when one considers the error bars as well. The error of the regression line is given by:

$$\boldsymbol{\sigma_y} = \mathbf{0}.0000647$$

Where the errors for the coefficients **A** and **B** are calculated using Equation **3-7** and **3-8** they calculated as:

$$\boldsymbol{\sigma_A} = 0.0046776$$

And

$$\boldsymbol{\sigma_B} = 0.0000155$$

Together with the error, the reactivity coefficient is then

$$\boldsymbol{\alpha_F} = -0.00015 \pm 0.00002$$

Similarly to the analysis made in the previous calculations, if one considers only the first two data points, then the value is -0.00014 which is nine times that of the error of $\boldsymbol{B}$, and if one considers the first and sixth points, the value is -0.00081 which 52 times that of the error in $\boldsymbol{B}$. Just like in the previous analysis, it might be best to use $\boldsymbol{B}$ with its error as determined by the linear least squares fit for the value because of the large factors in terms of the error in $\boldsymbol{B}$**.**

If one uses three times the error as a guide, then points 303 and 304 could be considered to be statistically equal to the value at 300.

The interpretation is then that given the statistical uncertainty of the Monte Carlo calculation, which then appears as 0.0000155 in the uncertainty of B, the reactivity can be negative or positive, within the bounds of $(-0.0000155, 0.0000155)$.

4.6.3 Moderator Temperature Coefficient

This set of calculations done was to calculate the moderator temperature coefficient, where all materials excluding the material that included the moderator had a constant temperature of $300\ K$. The material containing SiC also has carbon but was not included. The input can be seen in Figure 4-18.

```
% ----------------------------------------------------------------------
mat  m_00001  0.08725570  tmp= 301.00  moder  grph  6000  % inputmat id  51
   6000.03c  1.0000E+00
mat  m_00002  0.08725570  tmp= 301.00  moder  grph  6000  % inputmat id  52
   6000.03c  1.0000E+00
mat  m_00003  0.00001791  tmp= 300.00                     % inputmat id   2
   2003.03c  1.0100E-06
   2004.03c  1.0000E+00
mat  m_00004  0.00024050  tmp= 300.00                     % inputmat id  12
   2003.03c  1.0100E-06
   2004.03c  1.0000E+00
mat  m_00005  0.08725570  tmp= 301.00  moder  grph  6000  % inputmat id  53
   6000.03c  1.0000E+00
mat  m_00006  0.07090440  tmp= 300.00  moder uabc 92238 moder oabc 8016 % inputmat id  21
   6000.03c  1.6667E-01
   8016.03c  4.9981E-01
   8017.03c  1.9000E-04
  92235.03c  5.2224E-02
  92238.03c  2.8111E-01
mat  m_00007  0.05014700  tmp= 301.00  moder  grph  6000  % inputmat id   7
   6000.03c  1.0000E+00
mat  m_00008  0.09527920  tmp= 301.00  moder  grph  6000  % inputmat id   8
   6000.03c  1.0000E+00
mat  m_00009  0.09613680  tmp= 300.00                     % inputmat id   9
   6000.03c  5.0000E-01
  14028.03c  4.6111E-01
  14029.03c  2.3425E-02
  14030.03c  1.5460E-02
mat  m_00010  0.09527920  tmp= 301.00  moder  grph  6000  % inputmat id  10
   6000.03c  1.0000E+00
therm grph 301.0 gre7.00t gre7.04t
therm uabc u-o2.11t
therm oabc 301 o2-u.10t o2-u.11t
% ----------------------------------------------------------------------
```

Figure 4-18: Input file with an increase in moderator temperature.

Similar to the calculations on the fuel temperature coefficient, an observation of the effect of temperature was done using five different temperatures. As seen in previous calculations, these temperatures are utilised to provide a better understanding of the variation in temperature on the reactivity. The results are portrayed in

Table **4-27** and graphically portrayed in Figure 4-19.

Table 4-27: Results for moderator temperature changes.

File name	Temperature in K	k_{eff} Serpent	Standard deviation (σ)	Δk_{eff} in Serpent results
a010	300	1.48411	0.000063	reference
v061	301	1.48411	0.000063	0
v062	302	1.48415	0.000062	-4
v063	303	1.48432	0.000063	21
v064	304	1.48419	0.000063	8
v065	305	1.48427	0.000064	16

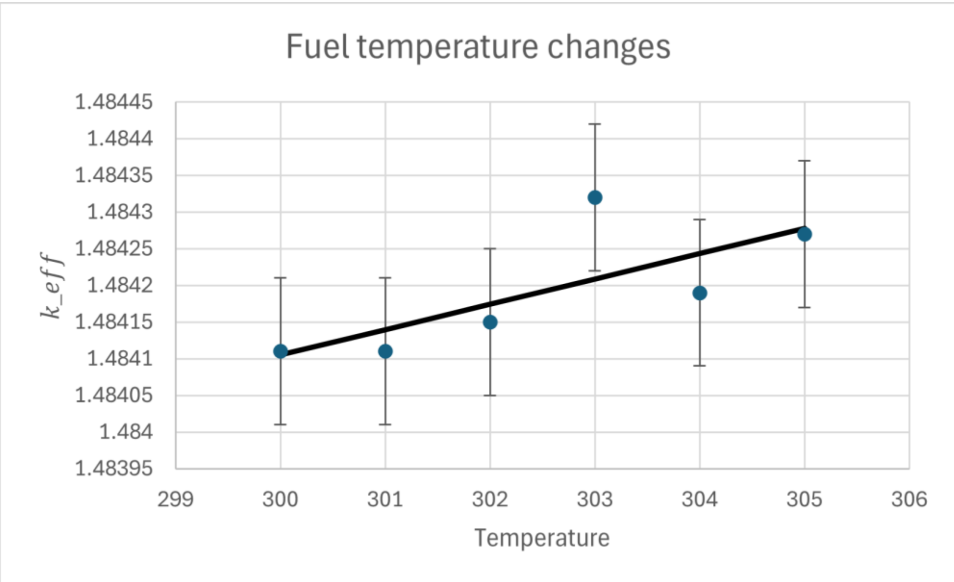

Figure 4-19: Figure displaying results for moderator temperature changes.

A linear fit with a residual of 0.000129 passes through all the points excluding at $T = 303\ K$, when one considers the error bars as well.

The reactivity coefficient, which is the slope of the line, is 0.0000346 resulting in the regression line given by:

$$y = 0.0000346x + 1.473734$$

The error of the regression line is given by:

$$\boldsymbol{\sigma_y} = \mathbf{0}.0000647$$

Where the errors for the coefficients **A** and **B** are calculated using Equation **3-7** and **3-8** and they are:

$$\boldsymbol{\sigma_A} = 0.0046776$$

And

$$\boldsymbol{\sigma_B} = 0.0000155$$

Together with the error, the reactivity coefficient is then

$$\boldsymbol{\alpha_M} = 0.000035 \pm 0.000015$$

If one considers only the first two data points, then the value is 0 and if one considers the first and sixth points, the value is -0.00016. However, the linearly fitted value of 0.00016 is the best value to select; it is also more conservative than 0 because when the value is taken to be 0, it will show that the k_{eff} will remain constant with every temperature change.

The corresponding value at temperature $300\,K$ is equal to that at $301\,K$ and if one uses three times the error as a guide, then the corresponding value at temperature $303\,K$ could be considered to be statistically equal to the value at $300\ K$ and $301\ K$.

A positive value for the moderator (graphite) for an HTGR can be expected, (Stacey W.M, 2018).

4.6.4 Neutron flux

Neutron flux graphs were plotted using the tally outputs of the calculations. The first set of graphs was plotted to reflect the neutron flux at the center of the reactor core at the isothermal temperatures $300\ K$ and $305\ K$, as highlighted in the figure below.

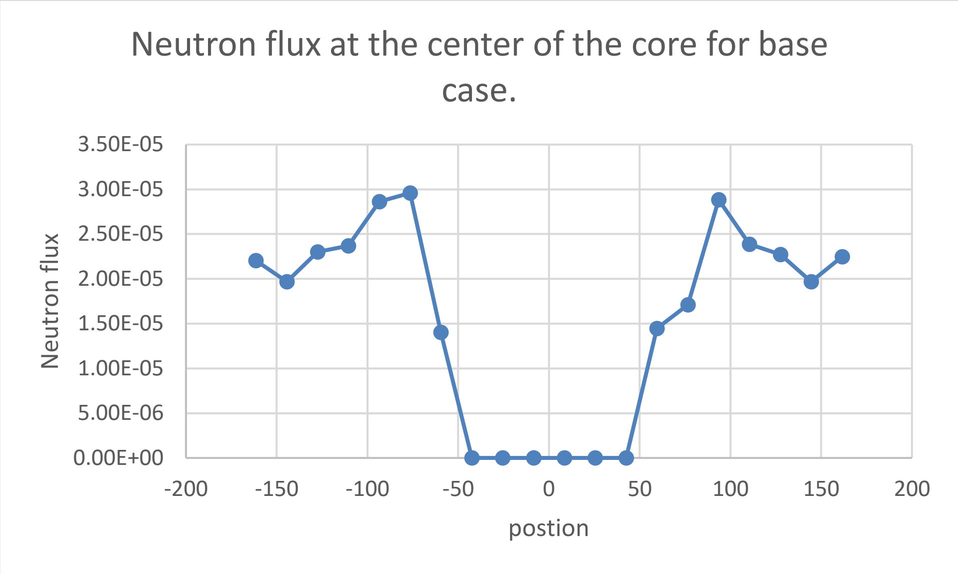

Figure 4-20: Neutron Flux at the Center of the Reactor Core from Reactor Core Tally Output for Temperature Isothermal Condition.

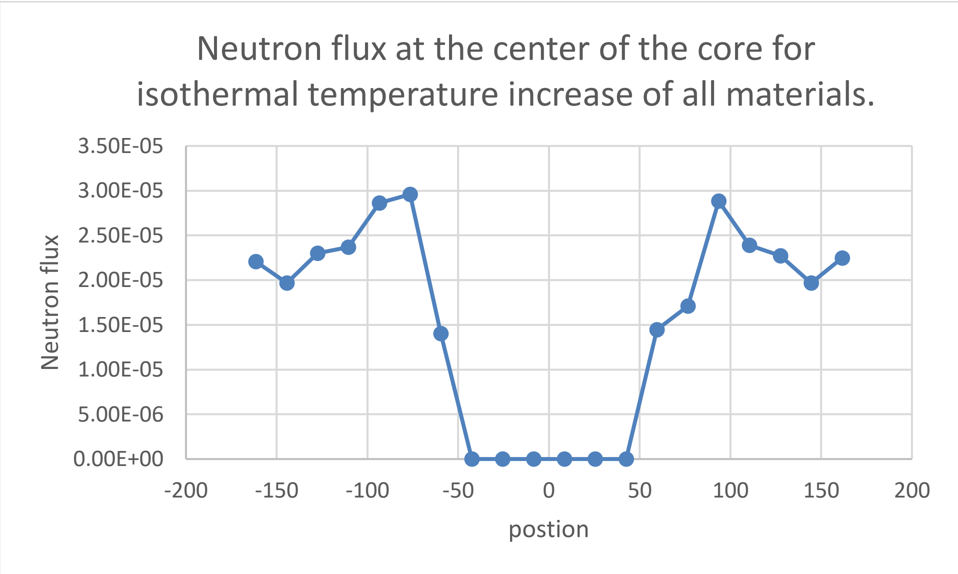

Figure 4-21: Neutron Flux at the Center of the Reactor Core from Reactor Core Tally Output for Isothermal Temperature Condition.

From the two figures above, not much difference can be seen from when the temperature is $T = 300\ K$ to when the temperature is $T = 305\ K$ both graphs have the same trajectory. To understand the shape of the plots, one needs to consider Fig 4.2 which is shown in this section again.

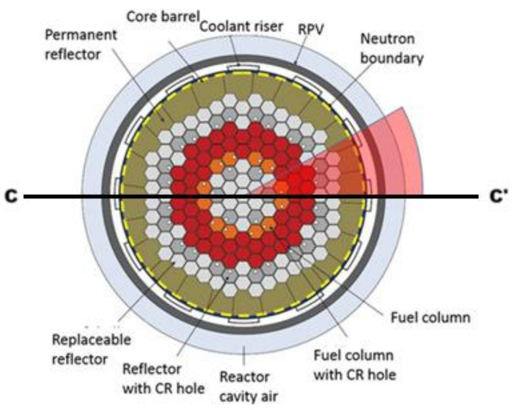

Figure 4-22: Full core Top view with horizontal line at center of the reactor.

The plot is taken through the horizontal line C C' shown in the figure. It is noted that in this section, there are no fuel blocks present at the centre of the core. Since the tallies collected were those of fission, the tallies should be zero at the centre, which is as observed in Figures 4.20 and 4.21.

The maximum percentage difference between the base case of $300\ K$ and isothermal temperature increase to $305\ K$ is 3.11%, meaning that there is little to no difference in the neutron flux for an isothermal condition when temperatures are changed from $T = 300\ K$ to $T = 305\ K$. Therefore all proceeding observations will only be based on temperatures $T = 305\ K$.

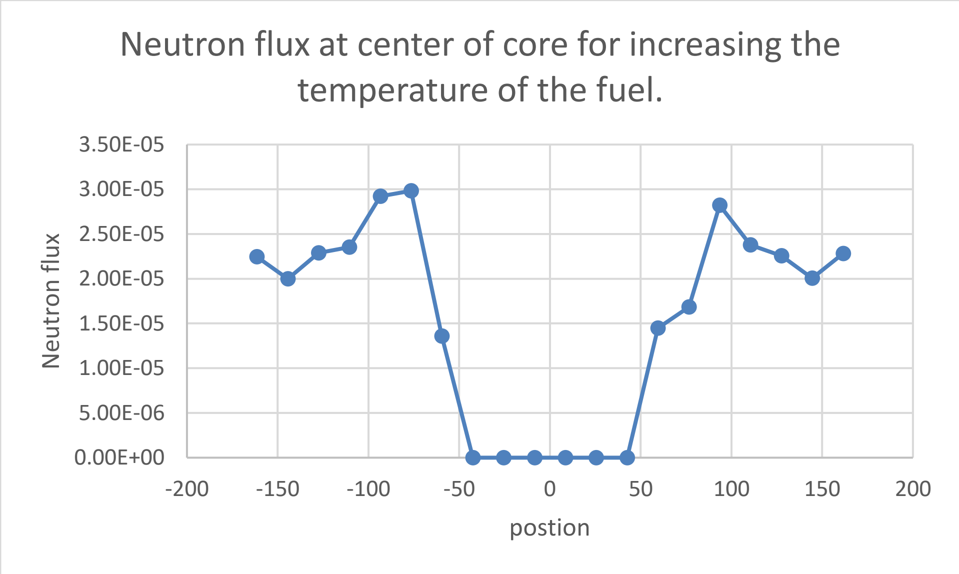

Figure 4-23: Neutron Flux at the Center of the Reactor Core from Reactor Core Tally Output For Temperature T=305 K Fuel Temperature Increase.

The maximum percentage difference between the base case of $300\ K$ and the case with fuel temperature $305\ K$ is 4.14%, meaning that there is little to no difference between the results from the base case.

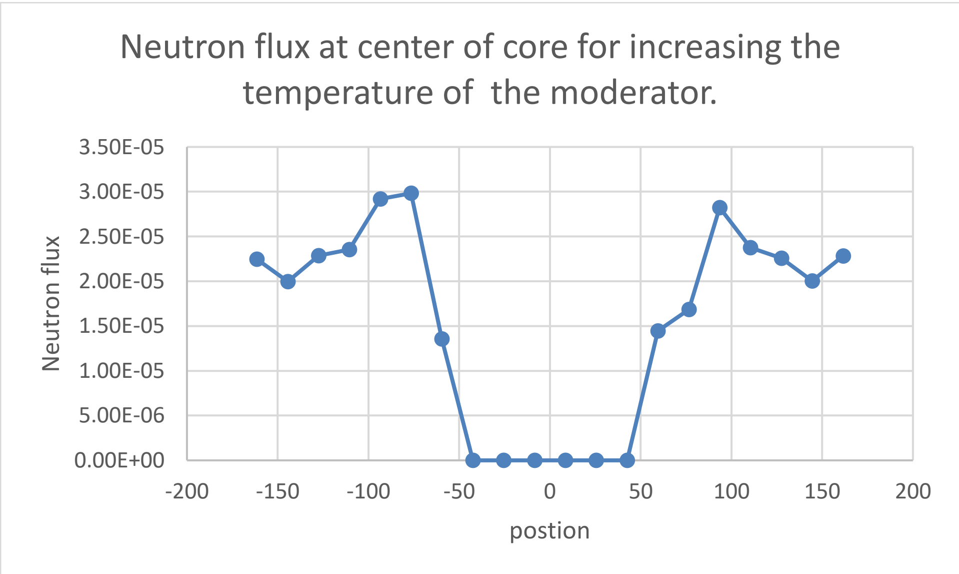

Figure 4-24: Neutron Flux at the Center of the Reactor Core from Reactor Core Tally Output For Moderator Temperature T=305 K Fuel Temperature Increase.

The maximum percentage difference between the base case of $300\ K$ and the case with $305\ K$ of the moderator temperature increase is 3.01% meaning that there is little to no difference with the results from the base case.

The figures above demonstrate a common trend to Figure 4-20 and Figure 4-21. Since the neutron flux is similar for all isothermal, fuel, or moderator temperature changes, a conclusion is that for all changes in temperature between $300\ K - 305\ K$, neutron flux at the center of the reactor core between positions $[-200{,}200]$ will remain within the same bounds as the original form of the base case, that is when $T = 300\ K$.

4.7 Comparative Analysis of Reactor Simulation Results

4.7.1 Comparison with Different Reactor Types

Although the MHTGR-350 reactor has not been widely analysed from a calculation point of view, numerous studies have used the Serpent and KENO-VI models to calculate safety parameters. In this section, the calculations and results received will be put into perspective with other existing literature by discussing the common trends of the model with other reactor types. These models are well known in reactor physics, hence they serve as a benchmark to judge the trends in safety parameters.

Bostelmann et al. (2016) does not only highlight the importance of cross-sections but also shows works like the one done in this dissertation where both Serpent and KENO-VI models are compared, but in her work, it is not the MHTGR-350 but the Very High Temperature Reactor Critical Assembly (VHTRC) being compared. In the comparison, it shows the difference in the multiplication factor between the outputs produced by the codes being within 300 - 500. Since this dissertation focusses on the modular HTGR then the difference in the multiplication factor should also lean toward those seen in Bostelmann et al. (2016), but in contrast, the results received seem to be deviating from the ones found in her work. It was identified in this work that the possible reason could be the geometry definition of the compositive hexagonal bodies in KENO-VI. This has been reported to the code developer of NWURCS for rectification.

Furthermore, there exist other papers such as Flouride-Salt-Cooled. (2016) whose focus was the consistency and accuracy of the Serpent and KENO-VI codes for the Flouride-salt-cooled High-temperature Reactors. The difference found in the results aligns with those seen in Bostelmann et al. (2016) with the small difference even though the reactors are not the same; this supports the notion that, irrespective of the design, the results should not lead to significant variations.

CHAPTER 5 CONCLUSION

The MHTGR-350 is a type of Generation-IV small modular reactor that’s been around for more than 40 years. The design of this compact reactor is distinguished by the inclusion of an advanced safety system. Numerous SMRs are under development and only two are operating, highlighting the stringent measures for licensing due to several nuclear accidents that framed the public perception of nuclear energy. This dissertation proposed the study of the MHTGR-350 by calculating and investigating the neutronics of a few safety parameters for regulatory research. To conduct this study, the use of computational tools along with existing research papers were used to create reliable results by exploring the relationships between the temperature and safety parameters.

The first set of calculations revealed large differences between the KENO-VI and Serpent results, causing an in-depth level-by-level analysis of the models. The most significant difference was observed at level 4, where lattices and units are located in the TRISO particle modelling. Although significant differences were observed at that level, the examination that was performed revealed no substantial discrepancies in both the lattices and units. This examination resulted in the conclusion that one of the models showed inaccurate results, the model was discovered to be the KENO-VI model because although it could run to completion, there were instances of ‘lost particles’. The possibility of removing this error is to model hexagonal bodies using planes instead of composite bodies (Ortensi *et al.*, 2015). This resulted in the Serpent model being used to perform neutronic calculations.

The calculations performed on the Serpent model included increasing the temperatures of all materials in the code isothermally, increasing the fuel temperature in the model, and increasing the temperature of the materials that included the moderator from $T = 300\ K$ to $T = 305\ K$. This results in a data set of 6 points. A linear fit to the results yielded a value of -0.00013 for the reactivity coefficient with a residual of 0.000156. A similar set of results was found for the fuel temperature. For the linear fit, a residual of 0.000129 was obtained and the reactivity coefficient (the Doppler coefficient) was calculated to be -0.00015. For the moderator temperature coefficients, for the six data points obtained, the residual was recorded as 0.000129, with the reactivity coefficient being 0.0000346. Although the coefficient of reactivity should be negative, the positive coefficient was not surprising, since it is known that, for a graphite moderator, this value can be positive (Stacey., 2018). The neutron flux for all the temperature changes of the materials mentioned in the previous section was also recorded using the tally output, and it was observed that for temperatures between $300\,K$ and $305\,K$ for all corresponding material temperature changes, the results are statistically equal at the centre of the reactor core.

CHAPTER 6 RECOMMENDATIONS FOR FUTURE WORK

This research has highlighted the importance of neutronic calculations by utilising safety parameters. However, not all safety parameters were included in this study. Therefore, future work that could be implemented for the MHTGR-350 would include the addition of more safety parameters to the neutronic study.

There were a few differences in the model given compared to that of Ortensi et al. (2015) some of which included the compacts of burnable poisons that are not homogenised materials and the random packing of coated particles, these are differences related to the design of the fuel compacts. Future research will be to build a model that incorporates the few differences.

Considering the unexpected deviation in the verification of the KENO-VI model, future work can consist of making use of the verification done in this study to find the underlying problem with the KENO-VI model and therefore construct research on neutronic study focused solely on the KENO-VI model. However, before this can be performed, the lost particles in the model must first be investigated. As explained in this work, a possible solution will be to use plane surfaces rather than composite bodies. In this way, each internal boundary would be defined by a single plane, and this would remove the possibility of neutrons entering undefined regions.

CHAPTER 7 REFERENCES

Aihara, J., Ueta, S., Honda, M., Blynskiy, P., Gizatulin, S., … Tachibana, Y. 2014. Development plan of high burnup fuel for high temperature gas-cooled reactors in future. Journal of Nuclear Science and Technology. 51(11–12):1355–1363.

Alhassan, E., Akaho, E.H.K., Ansah Adoo, N., Alhassan, E., Nyarko, B.J.B., … Della, R. 2010. Analysis of reactivity temperature coefficient for light water moderated HEU-UAl4 and LEU-UO2 lattices of MNSR. https://www.researchgate.net/publication/255685742.

Arostegui, D.A. 2019. Advanced Nuclear Reactors: Technology Overview and Current Issues. www.crs.gov.

Atkinson, S., Detkina, A., Litskevich, D. & Merk, B. 2021. A comparison of advanced boiling water reactor simulations between serpent/CTF and polaris/DYN3D: Steady state operational characteristics and burnup evolution. Energies. 14(4).

Benson, J. 2022. Nukes, Part 7, Micro Reactors. https://energycentral.com/c/pip/papers-directory-first-quarter-2022-update.

Bostelmann, F., Hammer, H.R., Ortensi, J., Strydom, G., Velkov, K. & Zwermann, W. 2016. Criticality calculations of the Very High Temperature Reactor Critical Assembly benchmark with Serpent and SCALE/KENO-VI. Annals of Nuclear Energy. 90:343–352.

Brey, H. L. (2001). Development history of the gas turbine modular high temperature reactor (IAEA Document No. XA0103026).

CEA (2015) e-DEN Neutronics. Monograph. Nuclear Energy Division, Commissariat à l'énergie atomique et aux énergies alternatives. ISBN 978-2-281-11372-3.

Cheng, Y., Zhou, Q., Zhu, Q., Xia, Z., Ning, T. & Zhang, Z. 2024. Research on the Source Convergence Diagnose Method of Monte Carlo Critical Calculation for Loosely Coupled System. EPJ Web of Conferences. 302:04012.

Dokhane, A., Ferroukhi, H., Zimmermann, M.A. & Aguirre, C. 2006. Spatial and model-order based reactor signal analysis methodology for BWR core stability evaluation. Annals of Nuclear Energy. 33(16):1329–1338.

Flouride-Salt-Cooled, H.-T.R. 2016. FHR Neutronics Benchmarking White Paper.

Fortini, A., Monteiro, F.B.A., Scari, M.E., Da Silva, F.C., Sousa, R. V., … Veloso, M.A.F. 2015. Recent advances on the use of reprocessed fuels and combined thorium fuel cycles in HTR systems. Progress in Nuclear Energy. 83:482–496.

Fridman, E., Duerigen, S., Bilodid, Y., Kotlyar, D. & Shwageraus, E. 2013. Axial discontinuity factors for the nodal diffusion analysis of high conversion BWR cores. Annals of Nuclear Energy. 62:129–136.

Gordon, T.L., Cooling, C.M., Williams, M.M.R. & Eaton, M.D. 2021. Numerical comparison of mathematical and computational models for the simulation of stochastic neutron kinetics problems. Annals of Nuclear Energy. 157.

GP Nyalunga. 2016. Developing a fresh core neutronic model at 300K for a VVER-1000 reactor type using MCNP6.

Gu, Z. (2018) History review of nuclear reactor safety. Journal article. Annals of Nuclear Energy, 120, pp. 682–690.

Huda, M.Q., Rahman, M.M., Imtiaz, M.A. & Nguyen, K.C. 2011. Design studies of a typical PWR core using advanced computational tools and techniques. Annals of Nuclear Energy. 38(9):1939–1949.

IAEA. 2005. Chernobyl's Legacy: Health, Environmental and Socia-Economic Impacts and Recommendations to the Governments of Belarus, Russian Federation and Ukraine.

IAEA. 2010. IAEA Safety Standards Licensing Process for Nuclear Installations for protecting people and the environment No. SSG-12 Specific Safety Guide. http://www-ns.iaea.org/standards/.

IAEA. 2019. Site evaluation for nuclear installations : specific safety requirements. International Atomic Energy Agency.

Ibrahim, A.M., Mosher, S.W., Evans, T.M., Peplow, D.E., Sawan, M.E., … Heltemes, T. 2010. ITER NEUTRONICS MODELING USING HYBRID MONTE CARLO0 DETERMINISTIC AND CAD-BASED MONTE CARLO METHODS.

Ilas, G., Ilas, D., Kelly, P.R. & Sunny, E.E. 2012. NUREG/CR-7107 "Validation of SCALE for High Temperature Gas-Cooled Reactor Analysis". http://www.nrc.gov/reading-rm.html.

INL. 2011. Modular HTGR Safety Basis and Approach. http://www.inl.gov.

Jaradat, M.K., Alawneh, L.M., Park, C.J. & Lee, B. 2014. Application of nonlinear nodal diffusion method for a small research reactor. Annals of Nuclear Energy. 66:20–30.

John R. Taylor. 2022. An introduction to error analysis The study of uncertainties in physical measurements. 2nd Edition ed. New York: University Science Books.

Kim, J. & Kim, Y. 2020. Three-Dimensional Pin-Resolved Transient Diffusion Analysis of PWR Core by the Hybrid Coarse-Mesh Finite Difference Algorithm. Nuclear Science and Engineering. 194(1):1–13.

Kurosawa, M. 2005. TORT/MCNP coupling method for the calculation of neutron flux around a core of BWR. Radiation Protection Dosimetry. 116(1–4):513–517.

Lamarsh, J.R. & Baratta, A.J. 2014. Introduction to Nuclear Engineering . England: Pearson.

Laranjo De Stefani, G. (2017) Use of thorium for high temperature gas-cooled reactors. Conference paper. Associação Brasileira de Energia Nuclear (ABEN).

Lee, H., Kim, W., Zhang, P., Lemaire, M., Khassenov, A., … Lee, D. 2020. MCS – A Monte Carlo particle transport code for large-scale power reactor analysis. Annals of Nuclear Energy. 139.

Lemaire, M., Lee, H., Tak, N. Il, Lee, H.C. & Lee, D. 2017. Multi-physics steady-state analysis of OECD/NEA modular high temperature gas-cooled reactor MHTGR-350. Journal of Nuclear Science and Technology. 54(6):668–680.

Leppänen, J. & Dehart, M.D. 2009. HTGR Reactor Physics and Burnup Calculations Using the Serpent Monte Carlo Code. https://www.researchgate.net/publication/235958383.

Lomonosov, A. & Rosatom, R. 2021. Design Maturity and Regulatory Expectations for Small Modular Reactors Cooperation in Reactor Design Evaluation and Licensing Working Group-SMR Task Force and Licensing and Permitting Task Force Title: Design Maturity and Regulatory Expectations for Small Modular Reactors Produced by: World Nuclear Association.

Melikkendli, B. & Tombakoglu, M. 2024. Stochastic differential equations for non-analog Monte Carlo model of point kinetics equations. Progress in Nuclear Energy. 176.

Mourtzanos, K., Housiadas, C. & Antonopoulos-Domis, M. 2001. Calculation of the moderator temperature coefficient of reactivity for water moderated reactors. www.elsevier.com/locate/anucene.

Nagaya, Y. 2025. Review of JAEA's Monte Carlo codes for nuclear reactor core analysis. EPJ Nuclear Sciences & Technologies. 11:1.

Stacey, W.M. (2005) Nuclear reactor physics. 2nd edn. Weinheim: Wiley-VCH.

Nyalunga, G., Naicker, V. & du Toit, M. 2016. Developing skills for neutronic modelling of nuclear power reactors in South Africa. Journal of Energy in Southern Africa. 27(4):64–76.

Ortensi, J., Pope, M.A., Sen, S., Strydom, G., Seker, V., DeHart, M., Gougar, H.D., Ellis, C., Baxter, A., Downar, T.J., Vierow, K. and Ivanov, K. (2015) Prismatic coupled neutronics/thermal fluids transient benchmark of the MHTGR-350 MW core design. Conference paper. Presented at the 2011 ANS Annual Meeting, Hollywood, FL, 26–30 June. Idaho National Laboratory.

Pratama, A.L. & Irwanto, D. 2020. Study on the Effects of Enrichment and Fraction of Coated Fuel Particles on Fissile Utilization of 100 MWt Prismatic-type of High Temperature Gas Reactor. In: Vol. 1493. Journal of Physics: Conference Series. Institute of Physics Publishing.

Ringane, T.P. (2022) Developing a full core model of the North Anna Reactor using SCALE 6.2.3, NESTLE and MCNP 6.2. MSc thesis. North West University.

Saenko, V., Ivanov, V., Tsyb, A., Bogdanova, T., Tronko, M., … Yamashita, S. 2011. The Chernobyl Accident and its Consequences. Clinical Oncology. 23(4):234–243.

Schappel, D., Terrani, K., Snead, L.L. & Wirth, B.D. 2019. Modeling Radionuclide Release of TRISO Bearing Fuel Compacts During Post-Irradiation Annealing Tests.

Sihlangu, S., Hou, J., Reitsma, F., Naicker, V. V, Sihlangu, S.F., … Reitsma, F. 2021. Uncertainty Propagation for the HTTR in terms of the IAEA CRP on HTGR Uncertainty Analysis in Modelling. https://www.researchgate.net/publication/354178402.

Silady, F.A. and Millunzi, A.X. (2007) Safety aspects of the Modular High-Temperature Gas-Cooled Reactor (MHTGR). Technical report. General Atomics, San Diego, CA.

Stacey W.M. 2018. Nuclear Reactor Physics. John Wiley & Sons.

Strydom, G. 2020. Consistent multi-scale uncertainty quantification methodology for multi-physics modelling of prismatic HTGRs. (May).

Talamo, A. 2007. Analytical calculation of the fuel temperature reactivity coefficient for pebble bed and prismatic high temperature reactors for plutonium and uranium-thorium fuels. Annals of Nuclear Energy. 34(1–2):68–82.

The Daily Beast. 2017. Three Mile worker on how he survuved. The Daily Beast. https://www.thedailybeast.com/three-mile-island-worker-on-how-he-survived-nuclear-catastrophe/ Date of access: 27 Jan. 2025.

U.S. Department of Energy. s.a. Enhanced Safety of Advanced Reactors. U.S. Department of Energy – Office of Nuclear Energy. https://www.energy.gov/ne/enhanced-safety-advanced-reactors Date of access: 02 Aug. 2025.

U.S.NRC. 2022. Three Mile Island Accident.

Vaz, P. 2009. Neutron transport simulation (selected topics). Radiation Physics and Chemistry. 78(10):829–842.

VTT. 2022. Serpent. https://serpent.vtt.fi/serpent/users.htm Date of access: 13 Feb. 2025.

Wang, C., Sun, X. & Sabharwall, P. 2020. CFD Investigation of MHTGR Natural Circulation and Decay Heat Removal in P-LOFC Accident. Frontiers in Energy Research. 8.

Wells BE, Phillips NR & Geelhood KJ. 2021. Choose an item. TRISO Fuel: Properties and Failure Modes. https://www.ntis.gov/about.

Wieselquist, W.A. & Lefebvre, R.A. 2023. SCALE 6.3.1 User Manual.

Ye, L., Wang, M., Wang, X., Deng, J., Xiang, Y., … Su, G.H. 2020. Thermal hydraulic and neutronics coupling analysis for plate type fuel in nuclear reactor core. Science and Technology of Nuclear Installations. 2020.

Zohuri, B. 2017. Neutronic Analysis For Nuclear Reactor Systems Second Edition. 2nd ed. Springer International Publishing.

Zu, T., Tang, Y., Huang, Z., Qin, S., Li, J., … Wu, H. 2021. Treatments of Thermal Neutron Scattering Data and Their Effect on Neutronics Calculations. Frontiers in Energy Research. 9.